Diabetes-Associated Mutations in Human Insulin: Crystal Structure and Photo-Cross-Linking Studies of A-Chain Variant Insulin *Wakayama*[†,‡]

Zhu-li Wan,[§] Kun Huang,[§] Bin Xu,[§,||] Shi-Quan Hu,[§] Shuhua Wang,[§] Ying-Chi Chu,[⊥] Panayotis G. Katsoyannis,[⊥] and Michael A. Weiss*[,§]

Department of Biochemistry, School of Medicine, Case Western Reserve University, Cleveland, Ohio 44106-4935, and Department of Pharmacology and Biological Chemistry, Mt. Sinai School of Medicine of New York University, New York, New York 10029

Received November 16, 2004; Revised Manuscript Received January 19, 2005

ABSTRACT: Naturally occurring mutations in insulin associated with diabetes mellitus identify critical determinants of its biological activity. Here, we describe the crystal structure of insulin *Wakayama*, a clinical variant in which a conserved valine in the A chain (residue A3) is substituted by leucine. The substitution occurs within a crevice adjoining the classical receptor-binding surface and impairs receptor binding by 500-fold, an unusually severe decrement among mutant insulins. To resolve whether such decreased activity is directly or indirectly mediated by the variant side chain, we have determined the crystal structure of Leu^{A3}-insulin and investigated the photo-cross-linking properties of an A3 analogue containing *p*-azidophenylalanine. The structure, characterized in a novel crystal form as an R_6 zinc hexamer at 2.3 Å resolution, is essentially identical to that of the wild-type R_6 hexamer. The variant side chain remains buried in a nativelike crevice with small adjustments in surrounding side chains. The corresponding photoactivatable analogue, although of low affinity, exhibits efficient cross-linking to the insulin receptor. The site of photo-cross-linking lies within a 14 kDa C-terminal domain of the α-subunit. This domain, unrelated in sequence to the major insulin-binding region in the N-terminal L1 β-helix, is also contacted by photoactivatable probes at positions A8 and B25. Packing of Val^{A3} at this interface may require a conformational change in the B chain to expose the A3-related crevice. The structure of insulin *Wakayama* thus evokes the reasoning of Sherlock Holmes in "the curious incident of the dog in the night": the apparent absence of structural perturbations (like the dog that did not bark) provides a critical clue to the function of a hidden receptor-binding surface.

Insulin is a globular protein containing two chains, A (21 residues) and B (30 residues) (Figure 1A). Expressed as a single-chain precursor (proinsulin; *1*) and stored in the pancreatic β-cell as a zinc-stabilized hexamer (*2*), insulin plays a central role in the hormonal control of metabolism. Molecular mechanisms of its folding, processing, secretion, and receptor binding are incompletely understood and define active fields of investigation. "Experiments of nature" are provided by the mutant insulin syndromes: rare monogenic forms of diabetes mellitus associated with mutations in the human insulin gene (*3*). Three classes of amino acid substitutions have been identified, perturbing (i) intracellular trafficking of the variant proinsulin to the glucose-regulated secretory granule of the β-cell (*4*), (ii) proteolytic processing of proinsulin in the endoplasmic reticulum to yield the mature hormone (*5*−*7*), or (iii) the conformation or receptor-binding activity of the mutant insulin (*8*−*10*). This study focuses on insulin *Wakayama* (*9*), the least active among clinical variants (*3*) (Table 1).[1] Processed and secreted normally, insulin *Wakayama* contains a mutation at a conserved site in an α-helix (Val^{A3} → Leu; asterisks in Figures 1A and 2). A clinical mutation at the homologous position of human IGF-1[2] (V44M; Figure 2) likewise impairs its binding to the type

† Supported in part by grants from the National Institutes of Health to P.G.K. (DK56673) and M.A.W. (DK40949).

‡ The coordinates of Leu^{A3}-insulin have been deposited in the Protein Data Bank as entry 1XW7.

* To whom correspondence should be addressed. E-mail: michael.weiss@case.edu. Telephone: (216) 368-5991. Fax: (216) 368-3419.

§ Case Western Reserve University.

|| Present address: Division of Biological Sciences, University of California at San Diego, La Jolla, CA 92093.

⊥ Mt. Sinai School of Medicine of New York University.

[1] In addition to insulin *Wakayama*, other diabetes-associated substitutions in the mature hormone occur in the B chain: Phe^{B24} → Ser (insulin *Los Angeles*) and Phe^{B25} → Ser (insulin *Chicago*; *8*). By analogy to abnormal hemoglobins, the mutant insulins are designated by the city of residence of the affected proband (*3*). Whereas A3, B24, and B25 mutations impair insulin binding, the His^{B10} → Asp clinical mutation would enhance activity but is associated with hyperproinsulinemia due to mistrafficking of the variant proprotein (*4*). A preliminary account of the photo-cross-linking of photoactivatable A3, B24, and B25 analogues to the isolated secreted ectodomain of the insulin receptor has previously been published (*31*).

[2] Abbreviations: CD, circular dichroism; CR, cysteine-rich domain of the receptor α-subunit; DPI, *des*[B26−B30]insulin, a truncated analogue; DPI-amide, modified DPI analogue in which the truncated B chain contains a C-terminal amide; DTT, dithiothreitol; EM, electron microscopy; IGF-1, insulin-like growth factor I; IR, insulin receptor; IRα-N, polyclonal antibody that recognizes 20 amino-terminal residues of the α-subunit; NAv, NeutrAvidin; rms, root-mean-square; rmsd, rms deviation; UV, ultraviolet; WGA, wheat germ agglutinin. Amino acids are designated by standard three- and one-letter codes. Nonstandard amino acids are as follows: Abu, α-aminobutyric acid; Ail, *allo*-isoleucine; Nle, norleucine; Nva, norvaline; Pap, *p*-azido-Phe; Pmp, *p*-amino-Phe; Tle, *tert*-leucine. Nomenclature describing IR modular domains is as described previously (*35*, *91*). "Native" elements of insulin designate features of crystal structures (*12*) and may not correspond to its conformation in a receptor complex (*69*).

10.1021/bi047585k CCC: $30.25
Published on Web 03/08/2005

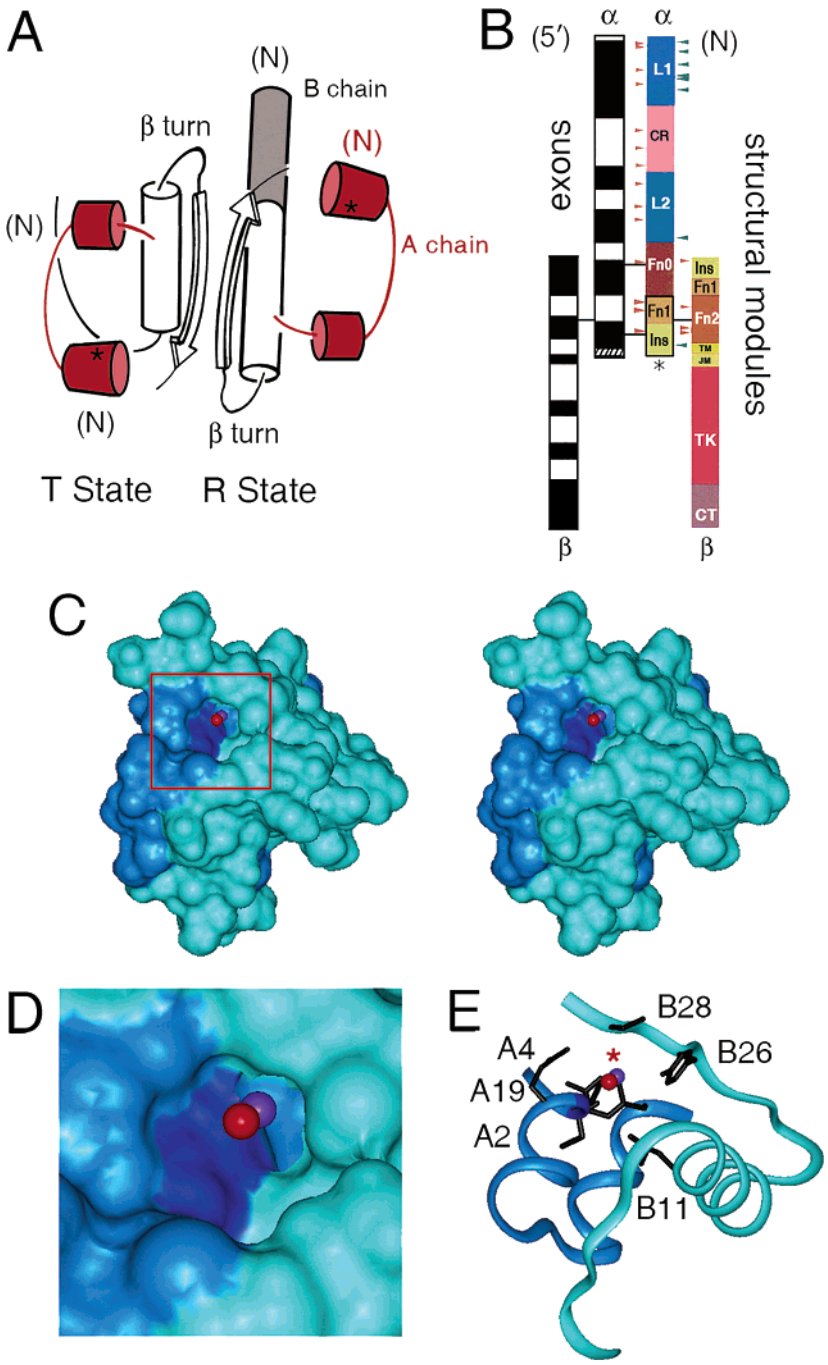

FIGURE 1: Insulin and the insulin receptor. (A) Cylinder model of insulin T- and R-state protomers. A chains are colored red and B chains white. The R-state-specific extension of the B-chain α-helix is colored gray. The asterisk denotes the position of the A3 side chain. (B) Putative domain structure of the IR (right) and corresponding organization of exons in the IR gene (left). Putative structural modules (L1, CR, L2, Fn0, and the N-terminal portion of Fn1-ID) are inferred from homology modeling (*35*). Orange arrowheads indicate sites of N-linked glycosylation; green arrowheads indicate sites of mutations that impair binding of insulin. The black box and asterisk indicate the 14 kDa fragment which contacts A3, A8, and B25. (C) Stereoview of Val^{A3} and the A3-related crevice in a T-state protomer (PDB entry 4INS). Residues surrounding Val^{A3} form a crevice within which the side chain of Val^{A3} is mostly buried (see Table 3A). Val^{A3} methyl groups (CPK representation) are partially (red ball) or completely buried (purple ball); methyl groups are more clearly visible in the enlargement in panel D. The A chain is colored dark blue and the B chain surface light blue. The portion in the red box is enlarged in panel D. (E) For clarity, a ribbon representation of insulin and side chains surrounding Val^{A3} is shown in the same orientation and color scheme as in panels C and D. The asterisk denotes the position of the A3 side chain.

I IGF receptor and is associated with severe growth- and mental retardation in utero and in childhood (*11*).

Val^{A3} is contained within the N-terminal α-helix of the A chain (residues A1−A8), an invariant feature of insulin-like folds (*12*−*16*), and an essential recognition element (*17*−*19*). The wild-type side chain packs within a nonpolar crevice between A and B chains that adjoins the classical receptor-binding surface (Figure 1C,D; *12*, *17*, *20*, *21*). Bordering this crevice are sequence-contiguous side chains Ile^{A2} and Glu^{A4}, the internal A6−A11 disulfide bridge, Tyr^{A19} and Leu^{B11} in the hydrophobic core, and Tyr^{B26} and Pro^{B28} projecting from an overlying B-chain "lid" (Figure 1E). Although substitution of valine by leucine would seem to be conservative or even stabilizing [as leucine exhibits a greater intrinsic

Table 1: Relative Receptor Binding Affinities of Insulin Analogues[a]

analogue	activity	analogue	activity
	(A) A3 Variants		
Gly^{A3}-insulin	0.09,[b,c] 0.2[d]	Ala^{A3}-insulin	1.8[b]
Abu^{A3}-insulin	1.8[b]	Nva^{A3}-insulin	1.4[b]
Ile^{A3}-insulin	11[b]	Leu^{A3}-insulin	0.18[b]
Ail^{A3}-insulin	18[b]	Tle^{A3}-insulin	36[b]
Trp^{A3}-insulin	3[f]	Thr^{A3}-insulin	13,[b] 50[e]
	(B) Photo-Cross-Linking Studies		
human insulin	100	Pmp^{A3}-t_A-insulin	3.0 ± 0.4 (3)
DKP-insulin[g]	161 ± 19 (4)	porcine Pmp^{A8}-t_A-insulin	52 ± 6 (3)
t_B-DKP-insulin	132 ± 5 (3)	Pmp^{B24}-t_B-DKP-insulin	59 ± 2 (3)
Pmp^{A3}-t_B-DKP-insulin	2.0 ± 0.2 (3)	Pmp^{B25}-t_B-DKP-insulin	147 ± 3 (3)
Pmp^{A14}-t_A-insulin	28 ± 3 (3)	Pmp^{A14}-t_B-insulin	74 ± 12 (4)

[a] Values are relative to human insulin, assumed to be 100%. The number in parentheses indicates the number of repetitions. Pmp analogues each contain a biotin tag attached to the α-amino group of B1 (designated t_B) or the ϵ-amino group of D-lysine substituted at the A1 position (t_A). [b] Data were obtained from ref *17*. N$^{\alpha}$Phe^{B1},N$^{\epsilon}$Lys^{B29}-Bisacetyl-insulin was used as a template for all A3 mutations tested in this study. Affinity results shown here are relative to this template, which exhibits 76% binding affinity. [c] Data were obtained from ref *90*. [d] Data were obtained from ref *89*, in which an engineered monomer (Glu^{B1},Glu^{B10},Glu^{B16},Glu^{B27},*des*B30)-insulin (4E insulin) was used as a template. The Gly^{A3} mutation exhibited 0.1% affinity, whereas the 4E template exhibited 47% affinity. [e] Data obtained from ref *83*. [f] Data obtained from ref *103*. [g] Value obtained from ref *43*. The placental membrane assay at 4 °C underestimates the activity of DKP-insulin relative to cell-based binding studies and lipogenesis assays at higher temperatures (*43*, *105*).

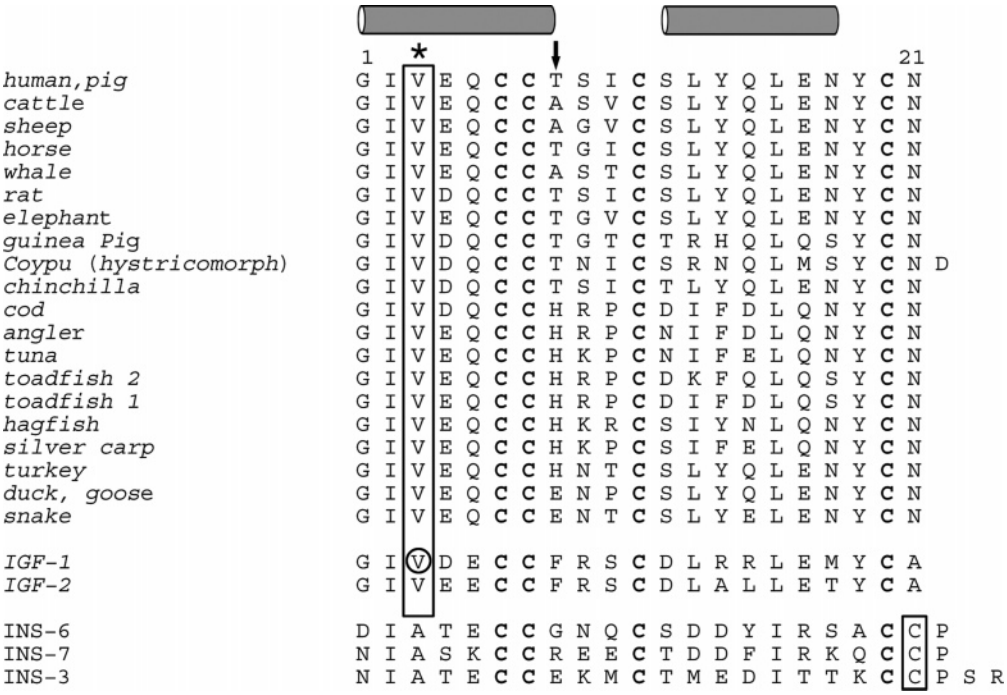

FIGURE 2: Sequences of insulin A chains (top group) in relation to the A domain of human IGF-1 and -2 (middle group) and representative *β*-class INS proteins of *C. elegans* (bottom group; *97*). Residues at position A3 are boxed (asterisk). The circled residue in IGF-1, V44, is a site of clinical mutation causing human dwarfism (V44M; *11*). Ancillary photo-cross-linking site A8 is denoted with an arrow; cysteines at positions A6, A7, A11, and A20 are shown in bold. Noncanonical cysteines in *C. elegans* sequences are boxed at the bottom right. Gray cylinders denote α-helices.

α-helical propensity than valine (*22*−*24*)], the activity of Leu^{A3}-insulin is impaired by 500-fold relative to that of native insulin (*17*). To investigate the molecular basis of such decreased activity, we describe the crystal structure of insulin *Wakayama* and investigate the cross-linking properties of a corresponding photoactivatable A3 analogue.

The structure of native insulin has been extensively characterized by X-ray crystallography (*12*, *20*, *25*−*27*)[3] and NMR spectroscopy (*18*, *28*, *29*).[4] Our study addresses whether the variant A3 side chain perturbs this structure. Our approach has two parts. The crystal structure of Leu^{A3}-insulin is first determined to visualize the A3-related crevice and neighboring receptor-binding surfaces. The structure, characterized by molecular replacement at 2.3 Å resolution, demonstrates that substitution of Val^{A3} with leucine is readily accommodated in an R_6 zinc hexamer (*26*). The substitution does not significantly affect zinc-mediated assembly or the

[3] Crystal structures of insulin as a zinc-free dimer (*27*) and as one of three types of zinc-stabilized hexamers (*25*, *26*) have been determined: T_6, $T_3R^f_3$, and R_6 (*108*). The T → R transition is characterized by a change in the secondary structure of the B1−B8 segment from extended (T state) to α-helix (R state) (see the gray shaded cylinder in Figure 1A). This reorganization is coupled to a change in configuration of Gly^{B8} and handedness of cystine A7−B7. Although the functional relevance of the R state is not well understood, it is possible that aspects of the T → R transition are recapitulated on receptor binding (*26*), including breakage of a T-state-specific interchain hydrogen bond (B25 NH···O═C A19; *12*, *67*) and a change in the conformation of Gly^{B8} (see the Discussion; *75*).

classical dimerization interface. Leu^{A3} remains almost completely buried in a nativelike crevice with only small adjustments in the positions of neighboring side chains. To investigate the potential role of the A3 side chain in the hormone−receptor complex, we next prepared a photoactivatable analogue containing *p*-azidophenylalanine (Pap; *30*, *31*) at this position. Packing of Pap^{A3} near the receptor is shown by its efficient cross-linking to the insulin receptor (IR; Figure 1B). Proteolytic mapping indicates that the site of cross-linking lies within a C-terminal 14 kDa fragment of the α-subunit also contacted by Pap probes at A8 and B25 (asterisk in Figure 1B; *32*, *33*). Because probes elsewhere in the B chain contact the N-terminal domain of the α-subunit (the L1 *β*-helix; Figure 1B) (*33*−*36*), we propose that insulin contains at least two distinct receptor-binding surfaces. Although this perspective is in overall accord with previous models (*37*, *38*), the pattern of specific contact points described here was unanticipated. Engagement of Val^{A3} at the receptor interface may require "opening" of the A3 crevice following induced fit of the B chain. This and related evidence suggesting that insulin adopts a novel conformation upon receptor binding is discussed in relation to the modular structure of the IR (*35*).

MATERIALS AND METHODS

Design of Insulin Analogues. Six analogues of human insulin were prepared by chain combination: Leu^{A3}-insulin for structural analysis and five Pap derivatives [positions A3 (in two versions), A8, B24, and B25]. Use of Pap extends the prior approach of Kursose et al. (*30*).[5] To facilitate characterization of photoproducts, B-chain Pap derivatives were modified by a biotinylamido-caproyl tag at the B-chain N-terminus (*30*), whereas A-chain derivatives contained an analogous tag at the ϵ-amino group of D-Lys^{A1} (substituted for the native glycine at position A1).[6] These tags are designated t_B and t_A, respectively (Table 1B). Leu^{A3}-insulin and the t_A-Pap^{A3} derivative were prepared using the native human B chain, whereas the monomeric "DKP" B chain was employed in syntheses of A3, B24, and B25 Pap derivatives; DKP indicates substitutions that hinder formation of dimers (Pro^{B28} → Lys and Lys^{B29} → Pro) and hexamers (His^{B10} → Asp) (*18*, *39*). For synthetic convenience, the t_A-Pap^{A8} analogue was prepared using a porcine B chain, obtained by sulfitolysis from porcine insulin. The human B-chain *S*-sulfonate was likewise obtained from recombinant human insulin, provided by Eli Lilly and Co. (Indianapolis, IN).

Synthesis of Insulin Analogues. The general protocol for solid-phase synthesis is as described previously (*40*). In brief, 4-methylbenzhydrylamine resin (0.6 mmol of amine/g; Bachem, Inc.) was used as solid support for synthesis of A-chain analogues; (*N-tert*-butoxycarbonyl-*O*-benzyl)threonine-PAM resin (0.56 mmol/g; Bachem, Inc.) was used as solid support for synthesis of B-chain analogues. A manual double-coupling protocol was followed (*41*, *42*). Protection of the *p*-NH_2 moiety of Phe (designated Pmp) was carried out by the 2-chlorobenzyloxycarbonyl group, which is stable under the conditions employed in the stepwise synthesis of A- and B-chain analogues. Chain recombination employed S-sulfonated B and variant A chains (approximately 2:1 by weight) in 0.1 M glycine buffer (pH 10.6) in the presence of dithiothreitol (*41*). Insulin analogues were isolated from the combination mixture (*42*) and purified as described previously (*43*); essentially native yields were obtained. Electrospray mass spectrometry (MS) in each case gave expected values and verified conversion of *p*-amino-Phe to Pap in the photoactivatable derivative (*30*). The purity was in each case greater than 98% as evaluated by analytical reverse-phase HPLC. MS revealed no anomalous molecular masses.

X-ray Crystallography. Crystals were grown by hanging-drop vapor diffusion in the presence of a 1:3.1 molar ratio of Zn^{2+} to protein monomer and a 3.9:1 ratio of phenol to protein monomer in Tris-HCl buffer as described previously (*44*). Drops consisted of 1 μL of protein solution (10 mg/mL in 0.02 M HCl) mixed with 1.5 μL of reservoir solution (0.02 M Tris-HCl, 0.05 M sodium citrate, 5% acetone, 0.03% phenol, and 0.01% zinc acetate at pH 8.2). Each drop was suspended over 1 mL of reservoir solution. A cosolvent (either acetone, phenol, or glycerol) was found to be essential for crystallization; in its absence, the protein forms an amorphous precipitate. Crystals (space group $P2_13$) were obtained at room temperature after 2 weeks. Data were collected from single crystals mounted in a rayon loop and flash-frozen to 100 K. Reflections from 50.1 to 2.3 Å were measured with a Bruker AXS CCD detector system using a rotating anode generator. Data were processed with *PROTEUM*. Leu^{A3}-insulin crystallized in a cubic unit cell containing an RR′ dimer in the asymmetric unit (unit cell parameters, $a = b = c = 70.85$ Å, $\alpha = \beta = \gamma = 90°$). An R_2 dimer derived from a rhombohedral R_6 crystal form of Asp^{B28}-insulin [Protein Data Bank (PDB) entry 1ZEG following removal of all water molecules, residues B27−B30, phenol, and zinc and chloride ions (*45*)] was used as a search model in molecular replacement using CNS (*46*). A translation-function search was performed using coordinates from the best solution for the rotation function following analysis of data between 15.0 and 4.0 Å resolution. Rigid-body refinement using CNS, employing overall anisotropic temperature factors and bulk-solvent correction, yielded values of 0.321 and 0.392 for R and R_{free}, respectively, for data between 50.1 and 3.0 Å resolution. Between refinement cycles, $2F_o - F_c$ and $F_o - F_c$ maps were calculated using data to 3.0 Å resolution; zinc and chloride ions and two phenols molecules were built into the structure using *O* (*47*). The geometry was continually monitored with *PROCHECK* (*48*); zinc ions and water molecules were built into the difference map as the refinement proceeded. Calculation of omit maps (especially in the first eight residues of the N-terminus of the B chain of each monomer) and further refinement were carried out using *CNS* (*46*), which implements maximum-likelihood torsion-angle dynamics and conjugate-gradient refinement. Statistics are provided in Table 2. Cavities and crevices in the protein structures were calculated with *SURFNET* (*49*).

[4] NMR analysis of an insulin monomer in aqueous solution at neutral pH requires protein engineering to limit self-association (*109*, *110*). Structures of such analogues resemble the crystallographic T state (*18*, *29*).

[5] Kurose et al. characterized a Pap^{B25} derivative of truncated insulin analogue *des*[B26−B30]insulin-amide (DPI-amide) containing a B1 biotin tag. The Pap moiety was found to cross-link in the segment of residues 704−718, which comprise the C-terminus of the α-subunit (*30*).

[6] The structure and function of insulin tolerate well the substitution of Gly^{A1} with D-amino acids (but not L-amino acids) (*111*, *112*); the crystal structure of one such analogue has been described previously (*113*).

Table 2: X-ray Diffraction and Refinement Statistics

resolution limits (Å)	50.1−2.3	highest-resolution shell	
R	0.205	resolution range (Å)	2.30−2.44
R_{free}	0.269	no. of reflections	758
R_{mere}		completeness (%)	95.2
all data	0.065	data redundancy	9.8
overall	23.52	R	0.305
highest-resolution shell	0.224	R_{free}	0.371
$I/\sigma(I)$	9.2	rmsd from standard geometry	
overall		bond lengths (Å)	0.010
no. of reflections used	5346	bond angles (deg)	1.4
completeness (%)	97.7	dihedral angles (deg)	21.0
data redundancy	12.9	improper angles (deg)	0.69
no. of protein atoms	812	structural rms deviations[a] (Å)	
no. of water molecules	85	molecule 1 vs molecule 2	
isotropic thermal model restraints (Å^2)		main chain	0.47
main chain bonds	1.39	side chain	1.25
main chain angles	2.69	variant vs wild type	
side chain bonds	2.16	main chain	0.68 ± 0.26
side chain angles	3.27	side chain	1.14 ± 0.34

[a] Values refer to pairwise alignment according to main chain atoms; additional statistical comparisons are provided in the Supporting Information. Molecules 1 and 2 refer to protomers of Leu^{A3}-insulin; the following line pertains to their mean similarity to a baseline collection of R-state structures (R_6 and $T_3R_3^f$ hexamers; PDB entries 1BEN, 1MPJ, 1G7A, 1LPH, 3MTH, 1EV3, 1TRL, 1ZNI, 1ZEH, 6INS, 1EV6, 1TM, 1ZNJ, and 1ZEG). The rmsd values within this collection are similar (Supporting Information), indicating that the variant structure falls within the expected range of conformational variability.

CD Spectroscopy. Spectra of biotin-tagged insulin derivatives containing the photostable precursor residue Pmp were obtained using an Aviv spectropolarimeter at 4 °C. Samples contained 25−50 μM protein in 10 mM potassium phosphate (pH 7.4) and 50 mM KCl.

Lectin Purification of the Insulin Receptor. The human IR was partially purified from Chinese hamster ovary (CHO) cells stably transfected to overexpress the B-splicing isoform (line P3-A; kindly provided by D. F. Steiner) (*50*). Methods of cell culture and wheat-germ agglutinin (WGA) purification were as described previously (*50*). Cells were detached using Hank's-based enzyme-free cell dissociation buffer (Invitrogen Life Technologies). Specific binding of insulin to the WGA-purified IR was verified with polyethylene glycol 8000 precipitation according to the method of Schäffer (*38*).

Receptor Binding Assays. Receptor binding assays (Table 1) were performed using a human placental membrane (*51*) as described previously (*43*). Relative activity is defined as the ratio of analogue to human insulin required to displace 50% of specifically bound human [^{125}I]insulin (Amersham). In all assays, the percentage of tracer bound in the absence of competing ligand was less than 15% to prevent ligand-depletion artifacts. Each determination was performed with three or four replicates; values are reported as the mean and standard deviation (see Table 1B).

Photo-Cross-Linking Studies. The WGA-purified IR was mixed in the dark with photoactive insulins labeled at the indicated positions at a concentration of 200 nM at 4 °C with gentle shaking overnight. Binding solutions were then transferred to a Costar assay plate (Corning Inc.) for ultraviolet (UV) irradiation. Short-wave UV (254 nm) generated from a Mineralight lamp (model UVG-54, UVP, Upland, CA) was used with an optimum exposure time of 20 s and a distance of 1 cm from the light source. After cross-linking, the hormone−receptor complex was reduced with dithiothreitol (DTT) and resolved by 10 to 20% gradient SDS−PAGE. The separated proteins were then blotted onto a nitrocellulose membrane. Cross-linked adducts were probed with NeutrAvidin (NAv; Pierce, Rockford, IL). To verify the identity of the IR α-subunit, gels were also probed with anti-IRα antiserum (IR$_\alpha$-N; Santa Cruz Biotechnology, Santa Cruz, CA), a polyclonal antibody that recognizes the 20 N-terminal residues of the α-subunit (i.e., the L1 domain). Sites of cross-linking in the IR were mapped by partial proteolysis to discrete regions of the α-subunit. This strategy in part takes advantage of previous characterization of chymotryptic sites (*33*, *52*, *53*).

Chymotrypsin Digestion. WGA-purified receptors were cross-linked with photoactive insulins and digested at 37 °C with 100 μg/mL chymotrypsin (Sigma, St. Louis, MO) in a solution of 50 mM HEPES (pH 7.4) containing 0.1% Triton X-100 and 0.11 M NaCl. Digestions were stopped at successive times by heating aliquots at 95 °C for 5 min. An equal volume of Laemmli sample buffer was added, and the mixtures were treated with 100 mM DTT. Digestion mixtures were analyzed with a 10 to 20% gradient gel (SDS−PAGE), blotting onto a nitrocellulose membrane, and probed with NAv or IR$_\alpha$-N as described above. Proteolytic mapping permitted specific cross-linking efficiencies to be estimated on the basis of observation of an SDS−PAGE mobility shift between native proteolytic fragments of the α-subunit and their corresponding A- or B-chain adducts. The ratio of shifted to unshifted bands was 20−30% (data not shown), indicating that the efficiency of photo-cross-linking is at least this high. Efficiencies might be higher if the WGA-purified IR were not completely active, since inactive receptors would only contribute to the unshifted bands.

Deglycosylation of the Insulin Receptor and Chymotryptic Fragments. Chymotryptic fragments of the Pap-cross-linked IR complexes were deglycosylated with peptide *N*-glycosidase F (N-Glycanase; Prozyme, San Leandro, CA). Samples were denatured at 95 °C for 5 min in 20 mM sodium phosphate (pH 7.5) containing 0.1% SDS and 50 mM β-mercaptoethanol prior to deglycosylation. Solutions were cooled to room temperature, and nonionic detergent NP-40 (final concentration of 0.75%) and N-Glycanase (1 milliunit/μg of receptor in the initial chymotryptic digestion) were added. Samples were incubated at 37 °C for 4 h. The reaction

was stopped by heating the mixture at 95 °C for 10 min. An equal volume of Laemmli sample buffer was added. Samples were reduced with 100 mM DTT prior to SDS−PAGE. Control deglycosylation of the intact α-subunit indicated complete conversion of the 135 kDa glycoprotein band to a 98 kDa band in accord with past studies (*54*).

Interpretation of Molecular Masses. A Pap^{B24} insulin derivative has previously been shown to cross-link within L1 domain residues 1−158 (*33*). The electrophoretic mobility of the B24-cross-linked N-terminally glycosylated chymotryptic fragment corresponds to a molecular mass of 47 kDa; following enzymatic deglycosylation, the apparent mass is 31 kDa (including the B-chain adduct). These masses suggest a fragment of ca. 250 residues containing four or five glycosylation sites (Figure 1B). The putative structure of the L1−CR−L2 region (as obtained by homology modeling; *35*) predicts prominent chymotryptic sites between residues 245 and 260 (sequence of YYHFQDWRCVNFSFCQ). Cleavage within this segment would yield (in the absence of glycosylation) 29−30 kDa fragments. C-Terminal chymotryptic fragments are identified on the basis of cross-linking to the Pap^{B25} insulin derivative, previously shown to contact residues 704−718 (*30*). Pap^{B25}-cross-linked chymotryptic fragments thus provide a fingerprint for cross-linking to the C-terminal tail of the α-subunit. Such fragments exhibit apparent masses of 34 and 20 kDa when glycosylated, which upon deglycosylation run as 23 and 17 kDa bands, respectively (inclusive of the B-chain adduct). The latter fragment corresponds to ca. 110−130 amino acids and so provides a probe for the C-terminal tail of the α-subunit derived from the putative Fn1/ID domain (asterisk in Figure 1B). The chymotryptic fragment is smaller than this domain (residues 590−731; 142 amino acids). The mass difference upon deglycosylation (3 kDa) indicates that the fragment contains at least one N-linked carbohydrate; the Fn1/ID region contains three N-linked sites of glycosylation (residues 605, 624, and 671).

RESULTS

Our study has two parts. The crystal structure of Leu^{A3}-insulin (insulin *Wakayama*) is first determined for the purpose of investigating the environment of the mutant side chain and evaluating whether transmitted changes occur in the conformation of adjoining receptor-binding surfaces. Photo-cross-linking studies of Pap^{A3} are then described to test whether the photoactivatable probe contacts the IR. Control Pap substitutions are employed as standards; these lie on the surface of the A chain (position A8; *32*) and at two diabetes-associated sites in the B chain (B24 and B25; *33*). Biotin tags were introduced during synthesis to facilitate detection of photo-cross-linked domains of the insulin receptor. Structural details of the Leu^{A3} hexamer and statistical analyses are further described in the Supporting Information.

Crystallographic Studies. Leu^{A3}-human insulin was crystallized as an R_6 zinc hexamer (Figure 3A) in a novel lattice containing an RR′ dimer (Figure 3B) in the asymmetric unit; the hexamer is generated by crystallographic symmetry. The structure was determined by molecular replacement using an R_2 structure as a search model (rhombohedral phenol insulin, PDB entry 1ZEG). The refined model of Leu^{A3}-insulin (determined to a resolution of 2.3 Å at 100 K) includes all residues in each chain and 85 water molecules per protein dimer. As expected, the hexamer contains six bound phenol molecules (two per asymmetric unit; Supporting Information); their positions and mode of binding are essentially identical to those observed in the wild-type R_6 zinc hexamer (*26*, *55*−*57*).[7] Representative regions of the $2F_o - F_c$ electron-density map are given as Supporting Information. The refined model exhibits an *R* factor of 0.205, and an R_{free} of 0.269; diffraction parameters, data-collection statistics, and additional *R* factors are given in Table 2.

The structures of the two protomers (designated molecules 1 and 2) are similar to each other and to the structures of native R-state protomers (Figure 4): no significant changes are observed in secondary structure, chain orientation, mode of assembly, or structure of Zn^{2+}-binding sites. Root-mean-square deviations (rmsds; Tables S1-A and S1-B of the Supporting Information) between molecules 1 and 2 are 0.47 Å (main chain) and 1.25 Å (side chains), respectively. Comparison between the variant protomers and wild-type R-state structures yields rmsd values (excluding A3) in the range of 0.38−0.93 Å (main chain) and 0.95−1.68 Å (side chains). These ranges are similar to those obtained in pairwise comparison between structures of native insulin in different crystal forms (Table S1-C of the Supporting Information).[8] Two Zn^{2+}-binding sites are each well defined without evidence of multiple ligand conformations (Supporting Information). Ligation is mediated by three symmetry-related His^{B10} side chains with Zn−N distances of 2.02 Å (molecule 1) and 2.03 Å (molecule 2); the remaining coordination site is in each case occupied by a presumed chloride ion with Zn−Cl distances of 2.41 and 2.31 Å, respectively (molecules 1 and 2).

Like Val^{A3} in wild-type insulin, the variant Leu^{A3} side chain projects from the nonpolar surface of an amphipathic α-helix (residues A1−A8) to pack within a crevice between chains (Figure 3C). The Ramachandran conformation of the helix resembles that of wild-type insulin (Supporting Information). The A3 side chains are in each case largely buried; solvent accessibilities in the isolated protomers are less than 10% (relative to the exposure of valine in an extended polypeptide; Table 3A). The neighboring Ile^{A2} side chain is also buried; its complete inaccessibility in Leu^{A3}-insulin (relative to that of wild-type insulin; Table 3A) reflects the more efficient occupancy of corresponding A3-related crevices by leucine. The respective conformations of the wild-type and variant A3 side chains permit the methyl groups of Val^{A3} and Leu^{A3} to occupy similar but not identical positions relative to the helical framework of the protein (highlighted in red in Figure 4); side-chain dihedral angles (χ_1 for Val^{A3} and χ_1 and χ_2 for Leu^{A3}) are given in Table 3B. The conformation of Ile^{A2} in the variant structure is consistent with wild-type structures (Table 3B). The α-helical main-chain geometry of the variant A1−A8 segment also re-

[7] The classical orientation of the bound phenol is stabilized in part by hydrogen bonds from the phenolic hydroxyl group to the carboxyl oxygen of Cys^{A6} and amide nitrogen of Cys^{A11}; these are unaffected by the A3 mutation.

[8] An estimate of the intrinsic variability among wild-type insulin crystal forms is provided by mean pairwise rms deviations, defined as the average of rmsd values obtained in systematic pairwise alignment of main chain atoms (Supporting Information). This measure provides a baseline for assessment of rms deviations between the variant and native structures.

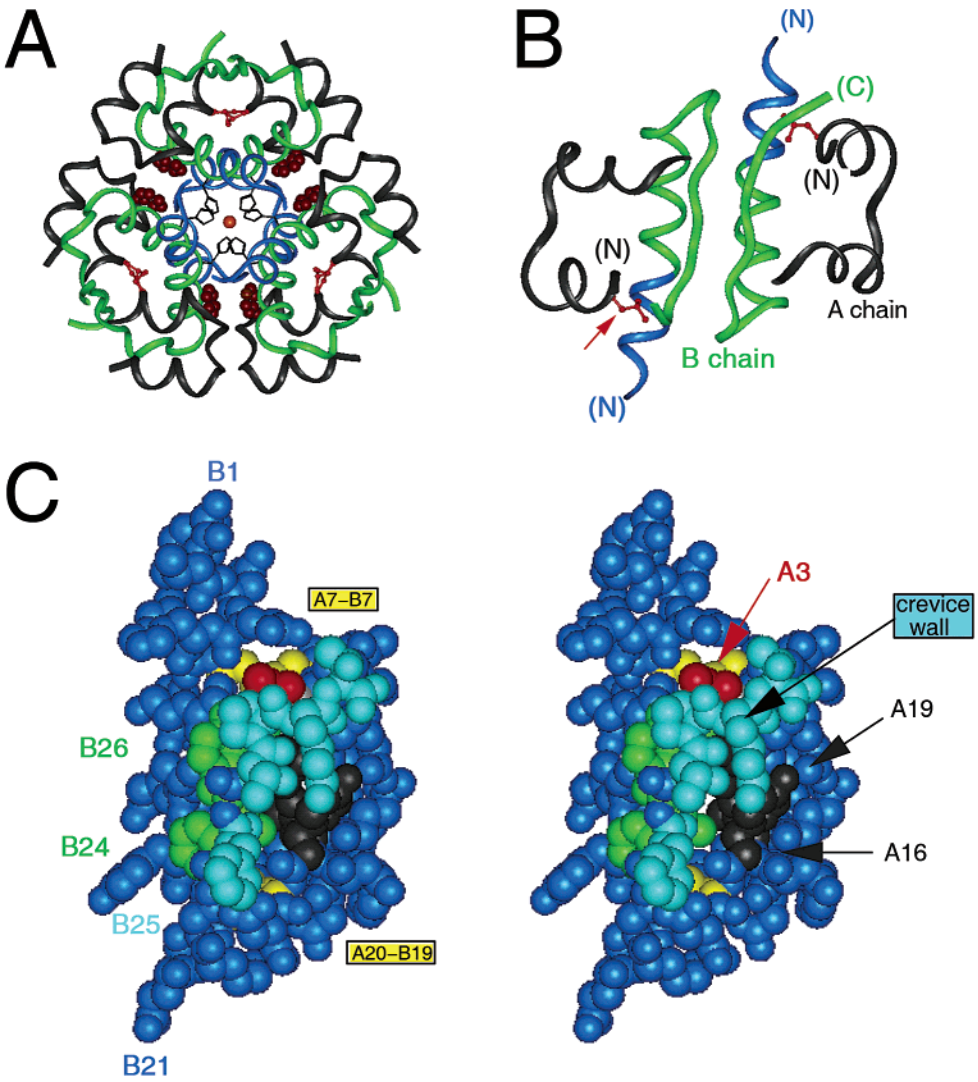

FIGURE 3: Crystal structures of insulin *Wakayama*. (A) Ribbon representation of the crystal structure of the R_6 hexamer of human Leu^{A3}-insulin. Zinc ion (orange sphere) and histidines (sticks) are shown at the center. The A chains of molecules 1 and 2 are colored black; the B chain is colored green, and phenol molecules are represented as bran spheres. The B-chain N-terminal (B1−B8) α-helix is colored blue, and the Leu^{A3} side chain is represented as red balls and sticks. (B) Ribbon model of the crystal structure of the human Leu^{A3}-insulin dimer. The color scheme follows that of panel A. (C) Stereoview of the surface representation of the crystal structure of human Leu^{A3}-insulin in the R-state protomer of molecule 1. The Leu^{A3} side chain is colored red. Disulfide bridges between residues A7−B7 and A20−B19 are colored yellow. Residues Leu^{A16} and Tyr^{A19} are colored black. Residues Phe^{B24} and Tyr^{B26} are colored green. Residues B26−B30 are colored light blue.

sembles that seen in wild-type R states.[9] The larger side chain volume of Leu^{A3} is well accommodated in the A3-related crevice without significant perturbations of surrounding side chains, including Ile^{A2}, cystines A6−A11 and A7−B7, Leu^{A16}, Tyr^{A19}, and Phe^{B24} (Figure 5). An adjustment is nonetheless apparent in the orientation of Tyr^{B26}, which immediately adjoins the site of substitution. The magnitude of the shift in the position of the phenolic oxygen (B26 O_ζ) is 0.64 ± 0.23 Å relative to wild-type R-state protomers. Since the B26 side chain can be deleted without loss of receptor binding activity (*58*, *59*), this small shift is unlikely to be biologically important. Similar small changes are observed in Leu^{A16} and Tyr^{A19}, but these are similar in magnitude to structural variations seen among wild-type crystal forms. The classical receptor-binding surface and hydrophobic core of insulin (*12*, *21*) are otherwise unaffected by the A3 substitution. The canonical disulfide bridges are likewise unperturbed.

Comparison of wild-type and variant protomers is aided by calculation of possible packing defects (cavities or crevices; *49*). Although the structures are well packed in each case, the dimensions of respective A3-related crevices may be estimated by the expendient of deleting the A3 side chain and calculating the volume of the crevice left behind (i.e., following rigid-body substitution of Leu^{A3} or Val^{A3} with glycine; calculations employed the structure described here and T- and R-state protomers obtained from PDB entries 4INS, 1ZNJ, and 1ZEG). Among wild-type structures, this procedure yields an A3 crevice volume of 97 ± 16 $Å^3$, whereas the corresponding volumes derived from Leu^{A3}-

[9] Among wild-type crystallographic protomers, the A1−A8 α-helix exhibits greater structural variability than do the other two helices. Such variability includes (a) a rigid-body translation and rotation of the helix as part of the T → R transition (*114*) and (b) local departures from ideal helical geometry (*12*). In the structure presented here, this α-helix exhibits distorted helical conformations in both molecules 1 and 2; the degree of distortion is consistent with wild-type structures.

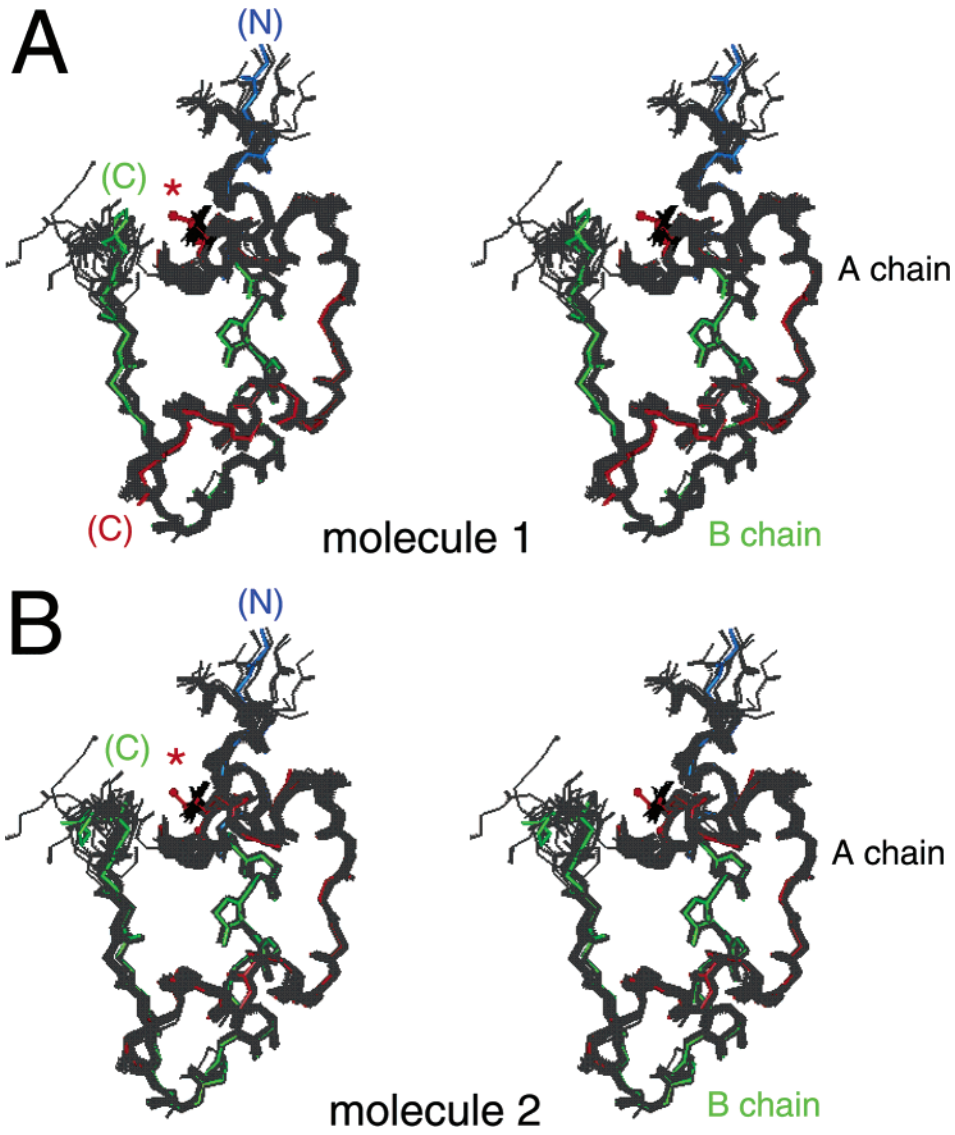

FIGURE 4: Comparison of the crystal structure of Leu^{A3}-insulin with that of insulin and insulin analogues in the R state. (A) R-State protomer of Leu^{A3}-insulin of molecule 1 in relation to an extensive set of crystal structures of insulin and insulin analogues (PDB entries 1EV3, 1EV6, 1MPJ, 1TRZ, 1TYL, 1MPJ, 1ZEG, 1ZEH, and 1ZNI). The A chain of Leu^{A3}-insulin is colored red (stick) and the B chain green (stick). The side chain of Leu^{A3} is colored red (ball and stick). Corystal structures of insulin and insulin analogues are colored black. Structures are aligned with respect to main-chain atoms of residues A2−A20 and B3−B28. (B) R-State protomer of Leu^{A3}-insulin of molecule 2 in relation to crystal structures of insulin and insulin analogues (PDB entries 1EV3, 1EV6, 1MPJ, 1TRZ, 1TYL, 1MPJ, 1ZEG, 1ZEH, and 1ZNI). The coloring scheme and alignment are the same as those in panel A.

insulin are 165 Å^3 (molecule 1) and 130 Å^3 (molecule 2). The increase is consistent with the standard volumes of amino acids [the volumes of Gly, Val, and Leu are 69, 140, and 166 Å^3, respectively (*60*)]. The difference in crevice volume between variant molecules 1 and 2, consistent with structural variability among wild-type protomers, reflects subtle differences in the positions of surrounding side chains. Relative to native insulin, such reorganization in each case serves, as expected, to enlarge the A3-related crevice to accommodate the larger A3 side chain. This repacking, necessary to prevent steric collision, does not require protrusion of Leu^{A3} into the solvent.

Photo-Cross-Linking Studies. To test whether residue A3 is near the IR, we synthesized an analogue containing Pap, a photoactivable derivative of phenylalanine (*61*). As previously described (*30*), Pap was chosen on the basis of its rigidity and small size (relative to other photoactivable moieties), thus limiting the distance range for cross-linking. The insulin derivative also contains a biotin tag tethered to the ϵ-amino group of D-Lys introduced at position A1.[6] The photo-cross-linking studies of the Pap^{A3} analogue were carried out in relation to previously characterized Pap analogues at positions A8, B24, and B25 (*32*, *33*). Following UV irradiation, the Pap^{A3} analogue exhibits rapid and efficient cross-linking to the WGA-purified IR (Figure 6A). At least 40% of these bound probes form covalent complexes as indicated by analysis of chymotryptic digests, an efficiency higher than that exhibited by Pap probes at A8, B24, or B25. Such photo-cross-linking is successively diminished by addition of native insulin, or at higher ligand concentrations, IGF-1, indicating that the Pap derivatives are binding to the specific hormone-binding pocket (data not shown). No competition is observed with unrelated proteins (hen egg white lysozyme, nonspecific immunoglobulins). In each case, no covalent complex is observed in the absence of irradiation or in control studies of the Pmp^{B25} precursor.

Table 3: Solvent Accessibilities and Conformation of A2 and A3 Side Chains

(A) Accessibilities

	residue A2		residue A3	
	main chain	side chain	main chain	side chain
variant molecule 1	3	0	0	8
variant molecule 2	0	0	0	6
wild-type T state[b]	10 ± 17	1 ± 1	<1	20 ± 9
wild-type R state[c]	44 ± 39	3 ± 3	<2	8 ± 8

(B) Conformations

	residue A2		residue A3	
	χ_1[a]	χ_2[a]	χ_1[a]	χ_2[a]
variant molecule 1	−169	165	−111	34
variant molecule 2	−172	169	−67	171
wild-type T state[b]	−63 ± 5	−173 ± 42	−167 ± 54	
wild-type R state[c]	−157 ± 63	174 ± 7	−175 ± 39	

[a] The χ_1 dihedral angle is ordinarily defined by atoms N, C^{α}, C^{β}, and C^{γ}. The χ_2 dihedral angle is defined by atoms C^{α}, C^{β}, C^{γ}, and C^{δ}. [b] Corresponding to the average and standard deviation among 13 T-state promomers of native insulin and insulin analogues (PDB entries 1BEN, 1G7A, 1LPH, 1MPJ, 1TRZ, 1TYL, 1TYM, 1ZNI, 3MTH, and 4INS). [c] Corresponding to the average and standard deviation among 15 R-state protomers of native insulin and insulin analogues (PDB entries 1BEN, 1EV3, 1EV6, 1G7A, 1LPH, 1MPJ, 1TRZ, 1TYL, 1TYM, 1ZNJ, 1ZEG, 1ZEH, and 3MTH).

To identify sites of cross-linking in the IR, we employed partial proteolysis with chymotrypsin to characterize fragments of the α-receptor subunit covalently bound to Pap-insulin derivatives (Figure 6B). Digestions were undertaken under native conditions, so fragments reflect accessible chymotryptic sites within and between structural modules of the receptor; approximate sites of preferential chymotryptic cleavage are indicated in Figure 6C (arrows; see Materials and Methods). An initial screen exploits the prior characterization of an N-terminal 47 kDa chymotryptic glycosylated fragment of the α-subunit by Pilch and colleagues (*53*) and the availability of antiserum to an N-terminal epitope (designated IR_{α}-N). On deglycosylation, the apparent mass of this fragment as determined by SDS−PAGE is 29−30 kDa (*31*) and so contains 250−260 amino acids. As previously described (*33*), analysis of limited chymotryptic digests demonstrates that Pap^{B24} contacts the N-terminal 47 kDa chymotryptic fragment, in accord with its binding to the L1 β-helix domain (lanes 3−6 in Figure 6B; *31*, *35*, *62*), the major hormone-binding region of the receptor (*63*, *64*). By contrast, probes at positions A3, A8, and B25 do not contact this N-terminal fragment but instead contact a distinct 34 kDa chymotryptic fragment (lanes 7−14 in Figure 6B and lanes 2, 5, and 8 in the top panel of Figure 6D), which must contain the C-terminal region of the α-subunit derived from the insert domain (residues 704−718) as indicated by prior cross-linking studies of a Pap^{B25} derivative (*30*). On further chymotryptic digestion, the 34 kDa fragment is cleaved to 20 kDa (lanes 2, 5, and 8 in the top panel of Figure 6D), which on deglycosylation yields a 17 kDa adduct (lanes 3, 6, and 9 in the top panel of Figure 6D). The digestion patterns of the A3, A8, and B25 cross-linked complexes are essentially identical, indicating that all three sites contact the C-terminal 14 kDa domain of the α-subunit.

Because the size of Pap exceeds the dimensions of the A3-related crevice, it is possible that the photo-cross-linking properties of the Pap^{A3} derivative do not reflect native contacts in the hormone−receptor complex. It is likely that the azido moiety protrudes beyond the solvent-accessible surface of native insulin. In addition, the D-Lys^{A1}-biotin and Pap^{A3} modifications might distort the structure of the A chain.[10] Further, the low receptor binding activity of the photostable precursor Pmp^{A3} analogue (∼11% relative to a control Pmp^{A14} analogue containing the same D-Lys^{A1}-biotin modification, Table 1) suggests that the photoreactive probe perturbs the hormone−receptor interface. Such impaired binding does not affect the high efficiencies of cross-linking that we have observed (as the photo-cross-linking reactions are performed at high concentrations of the ligand and receptor (200 nM) relative to the native dissociation constant (ca. 0.2 nM)) but may confound detailed interpretation of sites of cross-linking. That probes at A3 and A8 contact the same 14 kDa C-terminal fragment of the α-subunit is in accord with the presumed proximity of their azido groups in molecular models of the Pap variants (Figure 7B).

DISCUSSION

Disease-associated mutations in human proteins often provide important insight into structure−function relationships. Classical examples are provided by the hemoglobinopathies in which diverse substitutions in the α- or β-chains of hemoglobin A have been described in association with altered oxygen affinity, cooperativity, redox properties of the heme iron, and protein stability (for a review, see ref *65*). The insulinopathies have likewise provided novel insights into the biosynthesis, structure, and function of human insulin (*3*). Our study has focused on the structure of insulin *Wakayama*, a clinical variant remarkable for its very low affinity for the insulin receptor (*9*). As a seeming paradox, the mutation (Val^{A3} → Leu) interchanges branched-chain aliphatic residues within a nonpolar crevice. Such substitutions are generally well tolerated in proteins, and indeed, this structure is essentially identical to that of wild-type insulin. To rationalize the conservation of Val^{A3} (Figure 2) and low activities of Leu^{A3}-insulin and related analogues (Table 1; *17*, *66*), we and others have proposed that the A3-related crevice opens on binding to the insulin receptor to enable docking of Val^{A3} (and neighboring Ile^{A2}) within a nonpolar pocket of the receptor (Figure 7A; *44*, *66*−*69*). This model, which continues to be under active investigation as a working hypothesis, ascribes the impaired activity of insulin *Wakayama* to steric collision between Leu^{A3} and one face of the receptor. A direct contact between residue A3 and the IR α-subunit is supported herein by the high efficiency of cross-linking exhibited by a photoactivatable Pap^{A3} analogue. A related missense mutation has been identified at the homologous site in human IGF-I (Val44Met) in association with growth and developmental abnormalities (*11*).

[10] The capacity of the Pap^{A3} analogue to adopt a nativelike conformation is suggested by crystallization trials. Crystals of t_A-Pap^{A3}-insulin diffracting to 1.8 Å were grown by hanging-drop vapor diffusion under conditions similar to those used to obtain crystals of Leu^{A3}-insulin. The crystals belong to space group *R*3 (hexagonal unit cell dimensions of $a = b = 79.33$ Å and $c = 37.80$ Å) with one dimer per asymmetric unit. Possible Pap^{A3}-induced perturbations in the absence of Zn^{2+} and phenol are nonetheless suggested by CD spectra (Supporting Information). Their interpretation is uncertain, however, as similar perturbations are observed in the CD spectrum of KP-insulin (containing Pro^{B28} → Lys and Lys^{B29} → Pro substitutions; *115*) despite crystallographic verification of native secondary structure (*116*).

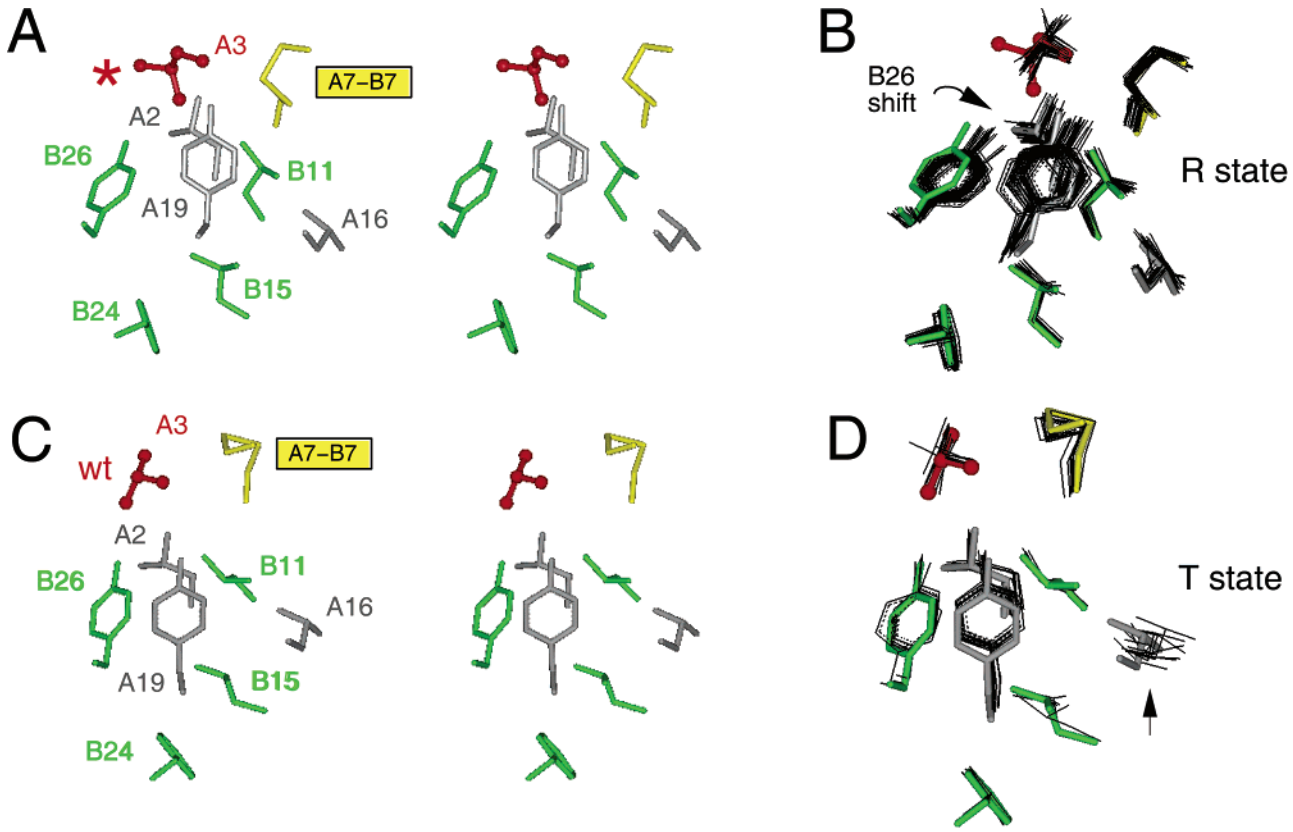

FIGURE 5: Packing schemes in the hydrophobic core. (A) Packing scheme of Leu^{A3}-insulin (molecule 1). Leu^{A3} is colored red, and residues Ile^{A2}, Leu^{A16}, and Tyr^{A19} are colored gray, residues Leu^{B11}, Leu^{B15}, Phe^{B24}, and Tyr^{B26} green, and residues Cys^{A7} and Cys^{B7} yellow. (B) Environment of Leu^{A3} in relation to a collection of prior R-state crystal structures. Insulin and insulin analogues (PDB entries 1EV3, 1EV6, 1MPJ, 1TRZ, 1TYL, 1MPJ, 1ZEG, 1ZEH, and 1ZNI) are colored black. The coloring scheme in panels B−D follows that of panel A. (C) Packing scheme of Val^{A3} in a representative T-state wild-type structure (PDB entry 4INS, molecule 1). (D) Comparison between the latter T-state structure and a collection of T-state protomers (PDB entries 1APH, 1BPH, 1CPH, 1DPH, 1G7A, 1TRZ, 1TYL, 1TYM, and 1ZNI), colored black.

The structure of Leu^{A3}-insulin as an R_6 hexamer (obtained in the presence of phenol and zinc ions) was determined in a cubic crystal (space group $P2_13$). To our knowledge, this crystal form has not previously been observed in crystallographic studies of wild-type human or porcine insulin. There are 24 molecules contained within the unit cell, forming 12 noncrystallographic dimers. The $P2_13$ unit cell contains a 3-fold symmetry axis running along one cubic diagonal. The 12 noncrystallographic dimers trimerize to form four crystallographic hexamers. This mode of lattice packing contrasts with standard rhombohedral insulin crystals in which the 3-fold axis of the hexamer is coincident with the crystallographic 3-fold axis as described among T_6, $T_3R_3^f$, and R_6 hexamers (*12*, *26*, *45*, *56*, *70*, *71*). Wild-type R_6 zinc−phenol−insulin hexamers have also been observed to crystallize in a monoclinic system (*26*, *56*, *57*, *70*). Structures of zinc−insulin hexamers are not significantly perturbed by lattice contacts, and indeed, the solution structure of an R_6 hexamer closely resembles crystallographic models (*72*−*74*). Likewise, the atomic-scale features of the Leu^{A3}-insulin appear not to have been influenced by the overall organization of the lattice in this novel cubic form.

The cubic R_6 crystal form was imposed by the contingencies of crystallization. Although the limited amount of synthetic material available prevented extensive trials, high-quality T_6 and $T_3R_3^f$ crystals of Leu^{A3}-insulin were not obtained under standard conditions. The reason for this is not clear given the evident structural similarity between the variant and wild-type insulins. Nevertheless, we do not believe that the R_6 crystal form has limited our view of the Leu^{A3} side chain and its environment. Despite structural differences between the T and R states (including the secondary structure of the B1−B8 segment, the conformation of the A7−B7 disulfide bridge, and subtle features of side chain packing; *25*, *26*), the environment of Val^{A3} is similar in the two types of protomers. The A3 side chain in each case projects from the N-terminal A-chain α-helix to contact the C-terminal β-strand within a corresponding crevice lined by Ile^{A2}, Glu^{A4}, Cys^{A6}, Cys^{A7}, Gln^{B4}, Cys^{B7}, Leu^{B11}, Tyr^{B26}, and Pro^{B28} (Figures 3C and 5 and the Supporting Information). It is therefore likely that the structural conservation of Leu^{A3}-insulin as observed in the structure presented here would extend to its environment in a T-state protomer. In the future, this inference can be tested through NMR studies of Leu^{A3} in the context of an engineered insulin monomer. The NMR structure of the related clinical variant of IGF-I (Val44Met) is similar to that of wild-type IGF-I (*11*).

It is not known which class of crystallographic protomer, T or R, more closely resembles the active conformation of insulin. Although the structure of an engineered insulin monomer in solution resembles the T state (*18*, *29*), it is possible that a change in structure occurs on receptor binding (for a review, see ref *35*). Although attention has been focused primarily on reorganization of the C-terminal B-chain β-strand as discussed in detail below (*67*, *69*), an R-like conformational change is also possible in the N-terminal

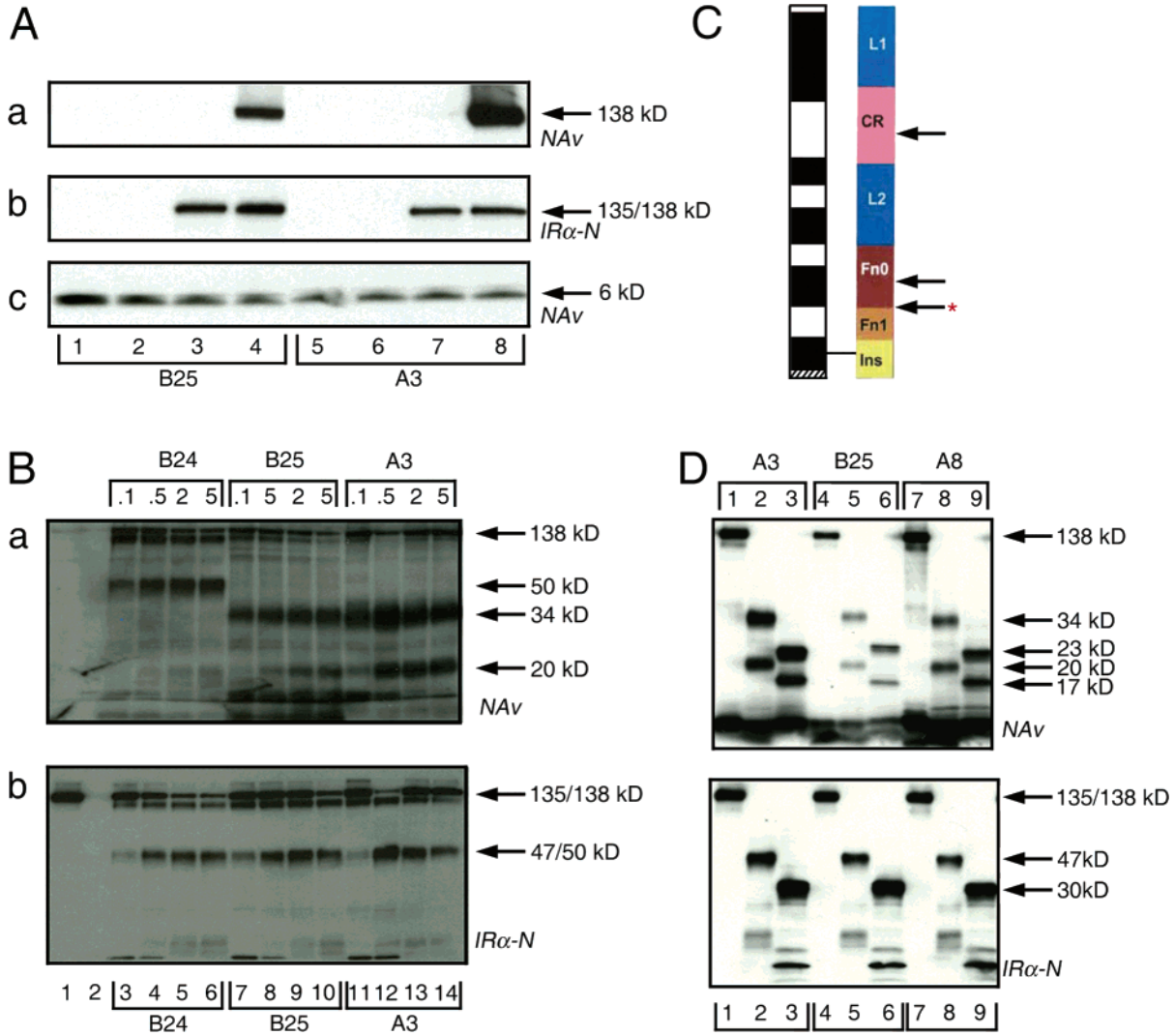

FIGURE 6: Photo-cross-linking and mapping. (A) Photo-cross-linking of Pap^{A3}-insulin and control Pap^{B25}-insulin analogue to lectin-purified IR. Analysis of photoproducts by SDS−PAGE and Western blot using NAv to detect the biotin tag on insulin (boxes a and c) or polyclonal antiserum IRα-N to detect the L1 domain (box b). Photo-cross-linking via positions B25 (lane 4) and A3 (lane 8) analyzed following DTT reduction. Lanes 1−3 and 5−7 contained control reaction mixtures in which either the IR was omitted (lanes 1, 2, 5, and 6) or samples were not irradiated (lanes 1, 3, 5, and 7). (b and c) Control blots to demonstrate that equal amounts of IR (b; with DTT) and insulin derivatives (c; without DTT) were present in each reaction mixture. (B) Mapping of hormone−receptor contacts by limited chymotryptic digestion. (a and b) Corresponding NAv-detected (a) and IRα-N-detected (b) blots following the initial digestion time course of B24-, B25-, and A3-cross-linked complexes. Lengths of digestion (minutes) are indicated at the top. Lane 1 in boxes a and b contained DTT-treated IR as a control, and lane 2 was blank. The molecular mass of the intact α-subunit is 135 kDa (including glycosylation; control lane 1 in panels A and B, only visible in panel B from the IRα-N detection). Limited chymotryptic digestion liberates a 47 kDa N-terminal domain (50 kDa, including the mass of the tethered B chain; lanes 3−6) and 34 kDa fragment (including the tethered A or B chain; lanes 7−14 in panel a) containing the C-terminal B25 contact site (704−718 peptide; *30*). The A3 digestion pattern (lanes 11−14 in panel a) mirrors that of the Pap^{B25}-cross-linked complex. B24 and B25 derivatives contain a biotin tag at the α-amino group of B1; the A3 derivative contains a biotin tag at D-Lys^{A1} (see Table 1). (C) Schematic outline of the α_2 dimer showing putative structural domains at right (L1, CR, L2, Fn0, and N-terminal portion of Fn1/ID) and sites of preferential chymotryptic cleavage of cross-linked hormone−receptor complexes (arrows). Additional central cleavage sites are possible but would not be probed by NAv−biotin adducts or IRα-N Western blot. The asterisk (red) denotes the site of photo-cross-linking by Pap^{B25} (*30*). Format is otherwise as in Figure 1B. (D) Further chymotryptic digestions of A3-, A8-, and B25-cross-linked complexes yield similar 20 kDa glycosylated C-terminal fragments (lanes 2, 5, and 8; including the mass of the tethered insulin A or B chain) that run as 17 kDa on deglycosylation (lanes 3, 6, and 9). Molecular masses are in each case shown at the right.

segment of the B chain (*12*, *66*). Indeed, recent studies of insulin by "chiral mutagenesis," D-amino acid substitutions at position B8 (an invariant glycine), have shown that stabilization of a native T-like monomer impairs receptor binding by 1000-fold (*75*).[11] These observations suggest that the hormone may adopt a non-T-state conformation at B8 on receptor binding. We imagine that the crystallographic T → R transition and induced fit of the insulin monomer, although distinct processes, will be found to exploit the same sites of flexibility in the N-terminal segment of the B chain. Resolving this issue will require cocrystallographic studies of a complex between insulin and the IR.

Role of Val^{A3} in Hormone−Receptor Recognition

Residues that are critically important to the function of insulin (including Val^{A3}; *17*) have been extensively investigated by mutagenesis and chemical modification (for a review, see refs *12* and *35*). A systematic overview has been provided by alanine scanning mutagenesis (*76*) and extended by chemical synthesis of selected analogues refractory to

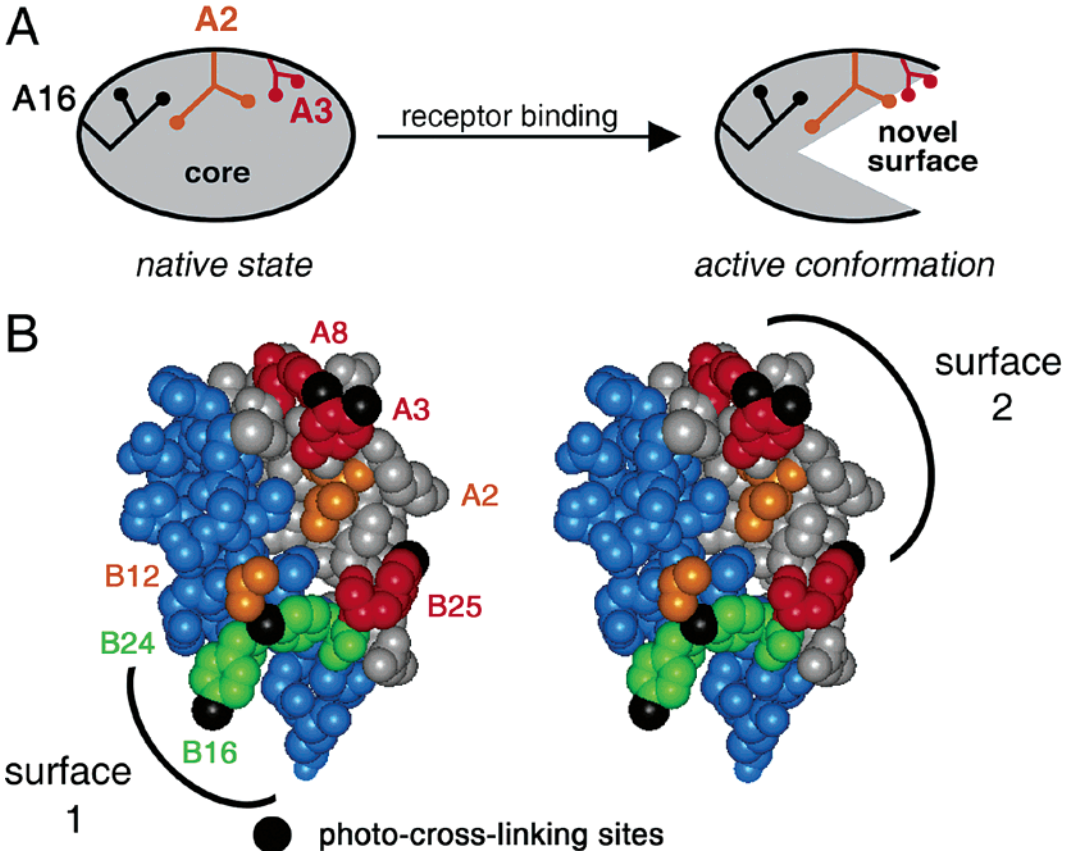

FIGURE 7: Induced fit and photo-cross-linking surface of insulin. (A) Schematic representation of the conformational change proposed to expose a hidden A-chain surface on receptor binding. Displacement or reorganization of the C-terminal segment of the B chain would expose Ile^{A2} and Val^{A3} (but not Leu^{A16}; *107*) to contact a nonpolar surface of the IR (*66*−*69*). (B) Five Pap variants were shown with the azido groups in black in a T-state protomer without the B26−B30 tail (PDB entry 4INS). The A chain is colored gray and the B chain blue. Three Pap positions on the same surface of the insulin molecule (A3, A8, and B25; surface 2) are colored red and were mapped to cross-linking of the C-terminus of the α-subunit. Two Pap positions on the same surface that cross-linked to the L1 domain (B16 and B24; surface 1) are colored green. Side chains of A2 and B12 are colored orange.

biosynthetic expression (*17*, *41*, *77*). These studies have yielded a trend: alanine substitutions that significantly impair activity occur at conserved sites, whereas well-tolerated substitutions occur at nonconserved sites. Such data do not in themselves distinguish between side chains that directly contact the receptor and side chains necessary for maintenance of an active overall structure. Although this distinction might seem apparent on the basis of the structural roles of conserved side chains in crystal structures, anomalies encountered in studies of structure−function relationships imply that neither the T nor R states can consistently rationalize effects of modifications as follows. These considerations are particularly important in relation to Val^{A3} since classical models (*20*, *21*) do not position this side chain at the receptor interface as visualized on the basis of low-resolution EM image reconstruction (*62*, *78*, *79*).[12]

Destabilization of a B-Chain Hinge Is Compatible with High Activity. Photo-cross-linking studies strongly suggest that Phe^{B24} and Phe^{B25} (like A3, sites of diabetes-associated mutations; ref *8*) contact the IR (*30*, *33*, *80*). Substitution of Phe^{B24} (which anchors the C-terminal β-strand to the core; *12*) with glycine, for example, leads to an altered B20−B30 segmental structure with near-native activity (*67*, *68*). Further, the activity of insulin is enhanced by chiral substitution of Phe^{B24} with D-Phe or D-Ala (*81*, *82*); these substitutions appear to be incompatible with the native structure of either crystallographic protomer. These results have led to a model in which the C-terminal B-chain β-strand reorganizes or detaches from the α-helical core of the hormone to contact the receptor. Because Pap probes at B24 and B25 contact different domains of the IR α-subunit (the N-terminal L1 β-helix and C-terminal insert domain-derived tail, respectively; *30*, *33*), we imagine that the strand inserts between these domains.

Partial Exposure of the Hydrophobic Core Rationalizes A-Chain Analogues. The induced fit of the C-terminal B-chain segment would expose Val^{A3} (and Ile^{A2}) to extend the receptor-binding surface of insulin (Figure 7A). The

[11] Chiral stabilization of an engineered insulin monomer (DKP-insulin; *18*) with a nonstandard Gly^{B8} → D-Ala^{B8} substitution leads to a 1000-fold decrease in the level of receptor binding despite retention of a native T-like solution structure (*75*, *117*). Because the activity of a related analogue containing a bulkier D side chain at B8 (*p*-amino-Phe) is reduced by "only" 200-fold, these decreases are likely to reflect impaired local flexibility rather than a steric clash with the IR. It is otherwise rare for mutation in the B chain to impair activity by more than 100-fold (*12*, *35*).

[12] In a model of a specific complex between insulin and the IR, Yip and colleagues interpreted EM images (*96*) to dock the T-state structure of insulin (crystallographic protomer 1BEN) within the interior of the ectodomain (*62*). In this model, Val^{A3} is not predicted to contact the IR whereas Thr^{A8}, Tyr^{B16}, and Phe^{B24} are each proposed to contact L1 domains. Although such B16 and B24 contacts are in accord with photo-cross-linking results (*33*, *36*), the Pap^{A8} derivative does not: it contacts the same C-terminal 14 kDa fragment of the IR α-subunit as Pap^{A3} and Pap^{B25} (see Figure 6D; *32*).

existence of a "hidden" A-chain functional surface is supported by the photo-cross-linking results presented here and the low activity of *allo*-Ile^{A2}-insulin, a chiral analogue whose "closed" structure is essentially unchanged from that of wild-type insulin (*44*, *69*). Inversion of chirality of the β-carbon of Ile^{A2} (*allo*-Ile) leads to subtle repacking of the hydrophobic core but without transmitted perturbations of the canonical protein surface. Stringent steric requirements of the hidden A-chain surface are further indicated by severe decreases in affinity incurred following subtle changes in side-chain shape or volume, such as Ile^{A2} → Leu, Val^{A3} → Leu, Val^{B12} → Leu, and Phe^{B25} → Leu (decreased by 22-, 555-, 33-, and 50-fold, respectively; ref *17*, *39*, *83*).

Tethered Single-Chain Insulin Analogues Exhibit Very Low Activities. Opening of the A3-related crevice on receptor binding is indirectly supported by the finding of nativelike structure in an inactive analogue (mini-proinsulin; *66*, *84*) in which the C-terminus of the B chain is tethered to the N-terminus of the A chain (*85*): the tether seals the A3 crevice and would hinder its exposure on receptor binding. Receptor binding is partially restored by increasing the tether length (*86*, *87*) or the number of residues in the connecting peptide (*88*).

The pattern of relative activities among A3 analogues suggests features of a cognate A3-binding pocket in the IR as follows. The low activities of Nva^{A3}-insulin (1.4%; Table 1A) and Leu^{A3}-insulin (0.18%) suggest that the A3 binding site in the α-subunit is structurally constrained. Packing defects at this interface, as might be associated with binding of Ala^{A3} and Abu^{A3} analogues, lead to destabilizing cavities. The steric stringency of the A3-binding pocket is not uniform in all directions as implied by the low but less impaired activities of Ail^{A3}, Ile^{A3}, Tle^{A3}, and Trp^{A3} analogues. Indeed, the very low activity of insulin *Wakayama* seems anomalous given that single methyl groups may be added to either branch of Val^{A3} (i.e., Ile^{A3} or Ail^{A3}) or at the β-carbon (Tle^{A3}) with a less than 10-fold decrease in the level of receptor binding (Table 1A). We speculate that the latter steric perturbations may individually be accommodated through local adjustments of the interface in a way that the concerted protrusion of Leu^{A3} cannot be. The extent of hydrophobicity of the putative A3-binding pocket is uncertain due to a conflict in the literature regarding the activity of Thr^{A3}-insulin (*17*, *83*). The very low activity of Gly^{A3}-insulin may reflect both loss of the A3 side chain and transmitted conformational perturbations (*89*, *90*).

Distinct Receptor Domains Contact Distinct Surfaces of Insulin

The IR is a receptor tyrosine kinase containing α- and β-subunits (*91*). Encoded by a single gene, the α-subunit binds insulin, whereas the transmembrane β-subunit contains a cytoplasmic kinase domain. Although the structure of the $\alpha_2\beta_2$ holoreceptor is not known, important insights have been obtained by sequence analysis and homology modeling (*35*, *92*). The α-subunit is a modular structure containing a series of distinct domains (Figure 1B; L1, CR, L2, Fn0, and the N-terminal portion of Fn1/ID). Mutagenesis and domain "swap" studies suggest that the major insulin-binding regions are contained within the L1 β-helix domain, the first fibronectin homology domain (Fn0), and the C-terminal tail derived from the ID (*63*, *93*, *94*). Additional contacts to the central L2 domain and fibronectin homology regions have been suggested by cross-linking studies (*30*, *95*). Specific binding of insulin to a 70 kDa monomeric minimized receptor containing the tripartite L1−CR−L2 fragment (CR, cysteine-rich domain) and Fn0 tethered to a C-terminal tail derived from the ID is observed (*94*).

Photo-cross-linking studies of Pap analogues suggest that insulin contains (at least) two distinct receptor-binding surfaces that contact distinct domains of the IR. Whereas probes at B16 and B24 contact the L1 β-helix of the α-subunit (residues 1−157; *33*, *36*), probes at A3, A8, and B25 contact the C-terminal 14 kDa domain (results presented here and refs *30* and *32*). The locations of these probes are shown in Figure 7B; residues B26−B30 have been removed to mimic their reorganization or displacement on receptor binding.[13] Interestingly, the two sets of probes project from opposing surfaces of insulin. EM studies suggest that the insulin molecule is engulfed within a large channel in the ectodomain of the $\alpha_2\beta_2$ holoreceptor (*96*), thus enabling multiple contacts at discrete surfaces. In this model, insulin employs major and minor receptor-binding surfaces to bind two α-subunits simultaneously as broadly envisaged on the basis of kinetic studies of analogues (*37*, *38*). In light of these models, it is possible that the Pap probes in the A and B chains are binding to different α-subunits. The conservation of A3, B24, and B25 among insulin-like growth factors and the tolerance of insulin to substitutions at B16 and A8 (*12*, *36*, *105*) suggest that the proposed binding surfaces also function in binding of IGF-I to the IR and type I IGF receptor and so cannot in themselves account for the distinct binding and signaling specificities of the two ligands (*106*).

We note that this and previous interpretations of photo-cross-linking experiments (*33*, *36*) implicitly assume that probes at various sites cross-link in the context of a single predominant mode of hormone binding. Although these conditions favor formation of a 1:1 high-affinity complex, it is formally possible that insulin binds to the holoreceptor in two or more ways related by a complex structural equilibrium. In one mode of binding, surfaces 1 and 2 may bind to the same α-subunit, for example, whereas in another mode, these surfaces may contact different subunits. It would be of interest in the future to synthesize photoactivatable insulin analogues containing two Pap substitutions to test whether both α-subunits can simultaneously be contacted. Since the efficiencies of photo-cross-linking are generally less than 40%, it is also formally possible that in these studies cross-linking by Pap^{A3} and the B-chain derivatives reflects different and mutually exclusive modes of binding, i.e., that side chains at A3 and B25 cannot simultaneously contact the C-terminal domain of the α-subunit. We consider this possibility to be unlikely as mutations at these sites (including those associated with diabetes) so markedly impair receptor binding affinity that A3 and B25 contacts must be integral to all modes of binding. Similar considerations apply to the issue of simultaneous contacts by B24 and B25 (*33*).

[13] Deletion of the five C-terminal residues of the B chain (residues B26−B30) prevents classical dimerization but is otherwise structurally well tolerated in the monomer (*118*, *119*). The analogue is a complete agonist in vivo (*120*) and on amidation of the B25 C-terminus exhibits native receptor binding affinity (*58*, *59*).

Concluding Remarks

This study has investigated the structure of a clinical variant of insulin with a substitution of Val^{A3} with leucine in a nonpolar crevice between A and B chains (insulin *Wakayama*; *9*). Although the substitution is well tolerated in the crystal structure (an R_6 zinc hexamer), the variant insulin exhibits markedly impaired biological activity and is associated with a monogenic form of diabetes mellitus (*3*). A variety of evidence, including high-efficiency cross-linking of a photoactivatable A3 derivative, suggests that on receptor binding insulin undergoes a change in conformation to open the A3-related crevice and enable Val^{A3} to dock at the hormone−receptor interface. We propose that larger side chains (such as Leu^{A3}) incur steric repulsion, rationalizing their reduced receptor binding affinities (*17*). Val^{A3} is conserved among vertebrate insulins and insulin-like growth factors (top and middle panels of Figure 2) but not among invertebrate insulin-like sequences; *Caenorhabditis elegans* INS sequences are shown in the bottom panel in Figure 2 (*97*). Divergence among invertebrate insulin-like proteins suggests that valine is not required at A3 for maintenance of an insulin-like fold (*16*), in accord with the nativelike structure of Leu^{A3}-insulin.

A limitation of this study is posed by the empirical coupling between insulin assembly and its crystallization. The structure presented here was determined in a hexamer, and the structure of the variant A3-related crevice is constrained by the classical dimer interface. Accordingly, it would be of future interest to investigate the solution structures of A3 analogues in an engineered insulin monomer. Such NMR studies could test whether the structure and stability of an insulin monomer are robust to changes in the size, shape, and polarity of the A3 side chain. In particular, because larger side chains (including Leu and Pap) can in principle protrude from the native protein surface to make contacts (favorable or unfavorable) not characteristic of the native complex, it would be of interest to extend this approach to substitutions similar or smaller in size but nonetheless incompatible with native function (Table 1). Such analogues would provide probes of the putative A3-binding pocket of the receptor.

In summary, the present study of insulin *Wakayama* and a related photo-activatable derivative provides evidence that a hidden non-polar surface of the A chain participates in receptor binding. Maintenance of native structure despite low activity extends a seeming paradox encountered in recent studies of A2 substitutions at a neighboring site in the hydrophobic core (*44*, *69*).[14] A definitive picture of the hormone−receptor complex awaits crystallographic analysis. Intriguing features of this complex have nonetheless emerged from EM image reconstruction and photo-cross-linking studies (for a review, see ref *35*). In particular, α-helices in both the A and B chains function to bind the IR but contact different domains of the modular α-subunit (*32*, *33*, *36*). Whereas the central α-helix of the B chain and Phe^{B24} engage its N-terminal domain (the L1 β-helix), the N-terminal A-chain α-helix and Phe^{B25} contact the C-terminal domain. It is possible that these domains are distant or flexibly linked in the free receptor but brought into well-ordered proximity on insulin binding. Insulin-directed structural reorganization of the α-subunit could provide an initial trigger for β-subunit signaling across the membrane and, if so, generalize the paradigm of hormone-induced dimerization of receptors observed among hematopoietic hormone and cytokines (*98*−*102*).

[14] The absence of structural perturbations among A2, A3, and B8 analogues (*44*, *69*, *75*) is reminiscent of a celebrated case of Sherlock Holmes ("Silver Blaze") in which a critical clue is provided by the anomaly of a dog undisturbed in the night (see Abstract; ref *121*).

ACKNOWLEDGMENT

We thank D. F. Steiner for the P3-A cell line overexpressing the IR and advice, Y.-M. Feng for porcine insulin, and T. L. Blundell, G. G. Dodson, P. De Meyts, M. Snider, Q. X. Hua, S. E. Shoelson, M. Shoham, J. Whittaker, J. Whittingham, and V. Yee for helpful discussion. Receptor binding assays were performed by S. Nakagawa in the Diabetes Research and Training Center at the University of Chicago (Chicago, IL).

SUPPORTING INFORMATION AVAILABLE

Five figures showing additional regions of the electron density map, alignment of molecules 1 and 2 of Leu^{A3}-insulin, and their structural relationship to the solution structure of an engineered insulin monomer, and two sets of tables providing structural comparisons between wild-type and variant crystal structures and inter-residue distances in the A3-related crevice. This material is available free of charge via the Internet at http://pubs.acs.org.

REFERENCES

1. Steiner, D. F., Cunningham, D., Spigelman, L., and Aten, B. (1967) Insulin biosynthesis: Evidence for a precursor, *Science 157*, 697−700.
2. Dodson, G., and Steiner, D. (1998) The role of assembly in insulin's biosynthesis, *Curr. Opin. Struct. Biol. 8*, 189−194.
3. Steiner, D. F., Tager, H. S., Chan, S. J., Nanjo, K., Sanke, T., and Rubenstein, A. H. (1990) Lessons learned from molecular biology of insulin-gene mutations, *Diabetes Care 13*, 600−609.
4. Carroll, R. J., Hammer, R. E., Chan, S. J., Swift, H. H., Rubenstein, A. H., and Steiner, D. F. (1988) A mutant human proinsulin is secreted from islets of Langerhans in increased amounts via an unregulated pathway, *Proc. Natl. Acad. Sci. U.S.A. 85*, 8943−8947.
5. Chan, S. J., Seino, S., Gruppuso, P. A., Schwartz, R., and Steiner, D. F. (1987) A mutation in the B chain coding region is associated with impaired proinsulin conversion in a family with hyperproinsulinemia, *Proc. Natl. Acad. Sci. U.S.A. 84*, 2194−2197.
6. Yano, H., Kitano, N., Morimoto, M., Plolonsky, K. S., Imura, H., and Seino, Y. (1992) A novel point mutation in the human insulin gene giving rise to hyperproinsulinemia (proinsulin Kyoto), *J. Clin. Invest. 89*, 1902−1907.
7. Warren-Perry, M. G., Manley, S. E., Ostrega, D., Polonsky, K., Mussett, S., Brown, P., and Turner, R. C. (1997) A novel point mutation in the insulin gene giving rise to hyperproinsulinemia, *J. Clin. Endocrinol. Metab. 82*, 1629−1631.
8. Shoelson, S., Haneda, M., Blix, P., Nanjo, A., Sanke, T., Inouye, K., Steiner, D., Rubenstein, A., and Tager, H. (1983) Three mutant insulins in man, *Nature 302*, 540−543.
9. Nanjo, K., Sanke, T., Miyano, M., Okai, K., Sowa, R., Kondo, M., Nishimura, S., Iwo, K., Miyamura, K., Given, B. D., et al. (1986) Diabetes due to secretion of a structurally abnormal insulin (insulin Wakayama). Clinical and functional characteristics of [Leu^{A3}] insulin, *J. Clin. Invest. 77*, 514−519.
10. Hua, Q. X., Kochoyan, M., and Weiss, M. A. (1992) Structure and dynamics of *des*-pentapeptide-insulin in solution: The molten-globule hypothesis, *Proc. Natl. Acad. Sci. U.S.A. 89*, 2379−2383.
11. Denley, A., Wang, C. C., McNeil, K. A., Walenkamp, M. J. E., van Duyvenvoorde, H., Wit, J. M., Wallace, J. C., Norton, R. S., Karperien, M., and Forbes, B. (2005) Structural and functional

characteristics of the Val44Met IGF-I missense mutation: Correlation with effects on growth and development, *Mol. Endocrinol. 19*, 711−721.
12. Baker, E. N., Blundell, T. L., Cutfield, J. F., Cutfield, S. M., Dodson, E. J., Dodson, G. G., Hodgkin, D. M., Hubbard, R. E., Isaacs, N. W., and Reynolds, C. D. (1988) The structure of 2Zn pig insulin crystals at 1.5 Å resolution, *Philos. Trans. R. Soc. London, Ser. A 319*, 369−456.
13. Eigenbrot, C., Randal, M., Quan, C., Burnier, J., O'Connell, L., Rinderknecht, E., and Kossiakoff, A. A. (1991) X-ray structure of human relaxin at 1.5 Å. Comparison to insulin and implications for receptor binding determinants, *J. Mol. Biol. 221*, 15−21.
14. Vajdos, F. F., Ultsch, M., Schaffer, M. L., Deshayes, K. D., Liu, J., Skelton, N. J., and de Vos, A. M. (2001) Crystal structure of human insulin-like growth factor-1: Detergent binding inhibits binding protein interactions, *Biochemistry 40*, 11022−11029.
15. Brzozowski, A. M., Dodson, E. J., Dodson, G. G., Murshudov, G. N., Verma, C., Turkenburg, J. P., de Bree, F. M., and Dauter, Z. (2002) Structural origins of the functional divergence of human insulin-like growth factor-I and insulin, *Biochemistry 41*, 9389−9397.
16. Hua, Q. X., Nakagawa, S. H., Wilken, J., Ramos, R. R., Jia, W., Bass, J., and Weiss, M. A. (2003) A divergent INS protein in *Caenorhabditis elegans* structurally resembles human insulin and activates the human insulin receptor, *Genes Dev. 17*, 826−831.
17. Nakagawa, S. H., and Tager, H. S. (1992) Importance of aliphatic side-chain structure at positions 2 and 3 of the insulin A chain in insulin-receptor interactions, *Biochemistry 31*, 3204−3214.
18. Hua, Q. X., Hu, S. Q., Frank, B. H., Jia, W., Chu, Y. C., Wang, S. H., Burke, G. T., Katsoyannis, P. G., and Weiss, M. A. (1996) Mapping the functional surface of insulin by design: Structure and function of a novel A-chain analogue, *J. Mol. Biol. 264*, 390−403.
19. Weiss, M. A., Hua, Q.-X., Jia, W., Chu, Y.-C., Wang, R.-Y., and Katsoyannis, P. G. (2000) Hierarchiacal protein "un-design": Insulin's intrachain disulfide bridge tethers a recognition α-helix, *Biochemistry 39*, 15429−15440.
20. Blundell, T. L., Cutfield, J. F., Cutfield, S. M., Dodson, E. J., Dodson, G. G., Hodgkin, D. C., Mercola, D. A., and Vijayan, M. (1971) Atomic positions in rhombohedral 2-zinc insulin crystals, *Nature 231*, 506−511.
21. Pullen, R. A., Lindsay, D. G., Wood, S. P., Tickle, I. J., Blundell, T. L., Wollmer, A., Krail, G., Brandenburg, D., Zahn, H., Gliemann, J., and Gammeltoft, S. (1976) Receptor-binding region of insulin, *Nature 259*, 369−373.
22. Lyu, P. C., Liff, M. I., Marky, L. A., and Kallenbach, N. R. (1990) Side chain contributions to the stability of α-helical structure in peptides, *Science 250*, 669−673.
23. O'Neil, K. T., and DeGrado, W. F. (1990) A thermodynamic scale for the helix-forming tendencies of the commonly occurring amino acids, *Science 250*, 646−651.
24. Padmanabhan, S., Marqusee, S., Ridgeway, T., Laue, T. M., and Baldwin, R. L. (1990) Relative helix-forming tendencies of nonpolar amino acids, *Nature 344*, 268−270.
25. Bentley, G., Dodson, E., Dodson, G., Hodgkin, D., and Mercola, D. (1976) Structure of insulin in 4-zinc insulin, *Nature 261*, 166−168.
26. Derewenda, U., Derewenda, Z., Dodson, E. J., Dodson, G. G., Reynolds, C. D., Smith, G. D., Sparks, C., and Swenson, D. (1989) Phenol stabilizes more helix in a new symmetrical zinc insulin hexamer, *Nature 338*, 594−596.
27. Badger, J., Harris, M. R., Reynolds, C. D., Evans, A. C., Dodson, E. J., Dodson, G. G., and North, A. C. (1991) Structure of the pig insulin dimer in the cubic crystal, *Acta Crystallogr. B47*, 127−136.
28. Hua, Q. X., and Weiss, M. A. (1991) Comparative 2D NMR studies of human insulin and *des*-pentapeptide insulin: Sequential resonance assignment and implications for protein dynamics and receptor recognition, *Biochemistry 30*, 5505−5515.
29. Olsen, H. B., Ludvigsen, S., and Kaarsholm, N. C. (1996) Solution structure of an engineered insulin monomer at neutral pH, *Biochemistry 35*, 8836−8845.
30. Kurose, T., Pashmforoush, M., Yoshimasa, Y., Carroll, R., Schwartz, G. P., Burke, G. T., Katsoyannis, P. G., and Steiner, D. F. (1994) Cross-linking of a B25 azidophenylalanine insulin derivative to the carboxyl-terminal region of the α-subunit of the insulin receptor. Identification of a new insulin-binding domain in the insulin receptor, *J. Biol. Chem. 269*, 29190−29197.
31. Xu, B., Hu, S. Q., Chu, Y. C., Wang, S., Wang, R. Y., Nakagawa, S. H., Katsoyannis, P. G., and Weiss, M. A. (2004) Diabetes-associated mutations in insulin identify invariant receptor contacts, *Diabetes 53*, 1599−1602.
32. Wan, Z., Xu, B., Huang, K., Chu, Y. C., Li, B., Nakagawa, S. H., Qu, Y., Hu, S. Q., Katsoyannis, P. G., and Weiss, M. A. (2004) Enhancing the activity of insulin at the receptor interface: Crystal structure and photo-cross-linking of A8 analogs, *Biochemistry 43*, 16119−16133.
33. Xu, B., Hu, S. Q., Chu, Y. C., Nakagawa, S. H., Whittaker, J., Katsoyannis, P. G., and Weiss, M. A. (2004) Diabetes-associated mutations in insulin: Consecutive residues in the B chain contact distinct domains of the insulin receptor, *Biochemistry 43*, 8356−8372.
34. Wedekind, F., Baer-Pontzen, K., Bala-Mohan, S., Choli, D., Zahn, H., and Brandenburg, D. (1989) Hormone binding site of the insulin receptor: Analysis using photoaffinity-mediated avidin complexing, *Biol. Chem. 370*, 251−258.
35. De Meyts, P., and Whittaker, J. (2002) Structural biology of insulin and IGF-I receptors: Implications for drug design, *Nat. Rev. Drug Discovery 1*, 769−783.
36. Huang, K., Xu, B., Hu, S. Q., Chu, Y. C., Hua, Q. X., Qu, Y., Li, B., S., W., Y., W. R., Nakagawa, S. H., Theede, A. M., Whittaker, J., De Meyts, P., Katsoyannis, P. G., and Weiss, M. A. (2004) How insulin binds: The B-chain α-helix contacts the L1 β-helix of the insulin receptor, *J. Mol. Biol. 341*, 529−550.
37. De Meyts, P. (1994) The structural basis of insulin and insulin-like growth factor-I receptor binding and negative co-operativity, and its relevance to mitogenic versus metabolic signalling, *Diabetologia 37* (Suppl. 2), S135−S148.
38. Schäffer, L. (1994) A model for insulin binding to the insulin receptor, *Eur. J. Biochem. 221*, 1127−1132.
39. Shoelson, S. E., Lu, Z. X., Parlautan, L., Lynch, C. S., and Weiss, M. A. (1992) Mutations at the dimer, hexamer, and receptor-binding, surfaces of insulin independently affect insulin-insulin and insulin-receptor interactions, *Biochemistry 31*, 1757−1767.
40. Merrifield, R. B., Vizioli, L. D., and Boman, H. G. (1982) Synthesis of the antibacterial peptide cecropin A (1−33), *Biochemistry 21*, 5020−5031.
41. Hu, S. Q., Burke, G. T., Schwartz, G. P., Ferderigos, N., Ross, J. B., and Katsoyannis, P. G. (1993) Steric requirements at position B12 for high biological activity in insulin, *Biochemistry 32*, 2631−2635.
42. Chu, Y. C., Hu, S. Q., Zong, L., Burke, G. T., Gammeltoft, S., Chan, S., Steiner, D. F., and Katsoyannis, P. G. (1994) Insulin-like compounds related to the amphioxus insulin-like peptide, *Biochemistry 33*, 11278−11285.
43. Weiss, M. A., Hua, Q.-X., Jia, W., Nakagawa, S. H., Chu, Y.-C., Hu, S.-Q., and Katsoyannis, P. G. (2001) Activities of monomeric insulin analogs at position A8 are uncorrelated with their thermodynamic stabilities, *J. Biol. Chem. 276*, 40018−40024.
44. Wan, Z., Xu, B., Chu, Y. C., Katsoyannis, P. G., and Weiss, M. A. (2003) Crystal structure of *allo*-Ile^{A2}-insulin, an inactive chiral analogue: Implications for the mechanism of receptor binding, *Biochemistry 42*, 12770−12783.
45. Whittingham, J. L., Edwards, D. J., Antson, A. A., Clarkson, J. M., and Dodson, G. G. (1998) Interactions of phenol and *m*-cresol in the insulin hexamer, and their effect on the association properties of B28 Pro → Asp insulin analogues, *Biochemistry 37*, 11516−11523.
46. Brunger, A. T., Adams, P. D., Clore, G. M., DeLano, W. L., Gros, P., Grosse-Kunstleve, R. W., Jiang, J. S., Kuszewski, J., Nilges, M., Pannu, N. S., Read, R. J., Rice, L. M., Simonson, T., and Warren, G. L. (1998) Crystallography & NMR system: A new software suite for macromolecular structure determination, *Acta Crystallogr. D54*, 905−921.
47. Jones, T. A., Zou, J. Y., Cowan, S. W., and Kjeldgaard, M. (1991) Improved methods for binding protein models in electron density maps and the location of errors in these models, *Acta Crystallogr. A47*, 110−119.
48. Laskowski, R. A., Macarthur, M. W., Moss, D. S., and Thornton, J. M. (1993) PROCHECK: A program to check the stereochemical quality of protein structures, *J. Appl. Crystallogr. 26*, 283−291.
49. Laskowski, R. A. (1995) SURFNET: A program for visualizing molecular surfaces, cavities and intermolecular interactions, *J. Mol. Graphics 13*, 323−330.
50. Yoshimasa, Y., Paul, J. I., Whittaker, J., and Steiner, D. F. (1990) Effects of amino acid replacements within the tetrabasic cleavage

site on the processing of the human insulin receptor precursor expressed in Chinese hamster ovary cells, *J. Biol. Chem. 265*, 17230−17237.

51. Cara, J. F., Mirmira, R. G., Nakagawa, S. H., and Tager, H. S. (1990) An insulin-like growth factor I/insulin hybrid exhibiting high potency for interaction with the type I insulin-like growth factor and insulin receptors of placental plasma membranes, *J. Biol. Chem. 265*, 17820−17825.
52. Boni-Schnetzler, M., Scott, W., Waugh, S. M., DiBella, E., and Pilch, P. F. (1987) The insulin receptor. Structural basis for high affinity ligand binding, *J. Biol. Chem. 262*, 8395−8401.
53. Waugh, S. M., DiBella, E. E., and Pilch, P. F. (1989) Isolation of a proteolytically derived domain of the insulin receptor containing the major site of cross-linking/binding, *Biochemistry 28*, 3448−3455.
54. Herzberg, V. L., Grigorescu, F., Edge, A. S., Spiro, R. G., and Kahn, C. R. (1985) Characterization of insulin receptor carbohydrate by comparison of chemical and enzymatic deglycosylation, *Biochem. Biophys. Res. Commun. 129*, 789−796.
55. Ciszak, E., and Smith, G. D. (1994) Crystallographic evidence for dual coordination around zinc in the T_3R_3 human insulin hexamer, *Biochemistry 33*, 1512−1517.
56. Whittingham, J. L., Chaudhuri, S., Dodson, E. J., Moody, P. C., and Dodson, G. G. (1995) X-ray crystallographic studies on hexameric insulins in the presence of helix-stabilizing agents, thiocyanate, methylparaben, and phenol, *Biochemistry 34*, 15553−15563.
57. Smith, G. D., Ciszak, E., Magrum, L. A., Pangborn, W. A., and Blessing, R. H. (2000) R_6 hexameric insulin complexed with *m*-cresol or resorcinol, *Acta Crystallogr. D56*, 1541−1548.
58. Cosmatos, A., Ferderigos, N., and Katsoyannis, P. G. (1979) Chemical synthesis of [*des*(tetrapeptide B27−30), Tyr(NH_2)26-B] and [*des*(pentapeptide B26−30), Phe(NH_2)25-B] bovine insulins, *Int. J. Protein Res. 14*, 457−471.
59. Fischer, W. H., Saunders, D., Brandenburg, D., Wollmer, A., and Zahn, H. (1985) A shortened insulin with full in vitro potency, *Biol. Chem. Hoppe-Seyler 366*, 521−525.
60. Zamyatnin, A. A. (1972) Protein volume in solution, *Prog. Biophys. Mol. Biol. 24*, 107−123.
61. Eberle, A. N., and de Graan, P. N. E. (1985) General principles for photoaffinity labeling of peptide hormone receptors, *Methods Enzymol. 109*, 129−157.
62. Yip, C. C., and Ottensmeyer, P. (2003) Three-dimensional structural interactions of insulin and its receptor, *J. Biol. Chem. 278*, 27329−27332.
63. Williams, P. F., Mynarcik, D. C., Yu, G. Q., and Whittaker, J. (1995) Mapping of an NH_2-terminal ligand binding site of the insulin receptor by alanine scanning mutagenesis, *J. Biol. Chem. 270*, 3012−3016.
64. Mynarcik, D. C., Williams, P. F., Schäffer, L., Yu, G. Q., and Whittaker, J. (1997) Identification of common ligand binding determinants of the insulin and insulin-like growth factor 1 receptors. Insights into mechanisms of ligand binding, *J. Biol. Chem. 272*, 18650−18655.
65. Perutz, M. F. (1979) Regulation of oxygen affinity of hemoglobin: Influence of structure of the globin on the heme iron, *Annu. Rev. Biochem. 48*, 327−386.
66. Derewenda, U., Derewenda, Z., Dodson, E. J., Dodson, G. G., Bing, X., and Markussen, J. (1991) X-ray analysis of the single chain B29-A1 peptide-linked insulin molecule. A completely inactive analogue, *J. Mol. Biol. 220*, 425−433.
67. Hua, Q. X., Shoelson, S. E., Kochoyan, M., and Weiss, M. A. (1991) Receptor binding redefined by a structural switch in a mutant human insulin, *Nature 354*, 238−241.
68. Ludvigsen, S., Olsen, H. B., and Kaarsholm, N. C. (1998) A structural switch in a mutant insulin exposes key residues for receptor binding, *J. Mol. Biol. 279*, 1−7.
69. Xu, B., Hua, Q. X., Nakagawa, S. H., Jia, W., Chu, Y. C., Katsoyannis, P. G., and Weiss, M. A. (2002) Chiral mutagensis of insulin's hidden receptor-binding surface: Structure of an *allo*-isoleucineA2 analogue, *J. Mol. Biol. 316*, 435−441.
70. Smith, G. D., and Ciszak, E. (1994) The structure of a complex of hexameric insulin and 4′-hydroxyacetanilide, *Proc. Natl. Acad. Sci. U.S.A. 91*, 8851−8855.
71. Smith, G. D., and Dodson, G. G. (1992) Structure of a rhombohedral R6 insulin/phenol complex, *Proteins 14*, 401−408.
72. Jacoby, E., Hua, Q. X., Stern, A. S., Frank, B. H., and Weiss, M. A. (1996) Structure and dynamics of a protein assembly. ^{1}H NMR studies of the 36 kDa R_6 insulin hexamer, *J. Mol. Biol. 258*, 136−157.
73. Chang, X., Jorgensen, A. M., Bardrum, P., and Led, J. J. (1997) Solution structures of the R_6 human insulin hexamer, *Biochemistry 36*, 9409−9422.
74. O'Donoghue, S. I., Chang, X., Abseher, R., Nilges, M., and Led, J. J. (2000) Unraveling the symmetry ambiguity in a hexamer: Calculation of the R_6 human insulin structure, *J. Biol. NMR 16*, 93−108.
75. Nakagawa, S. H., Zhao, M., Hua, Q. X., Hu, S. Q., Jia, W., and Weiss, M. A. (2005) Chiral mutagenesis of insulin. Foldability and function are inversely regulated by a stereospecific switch in the B chain, *Biochemistry* (in press).
76. Kristensen, C., Kjeldsen, T., Wiberg, F. C., Schaffer, L., Hach, M., Havelund, S., Bass, J., Steiner, D. F., and Andersen, A. S. (1997) Alanine scanning mutagenesis of insulin, *J. Biol. Chem. 272*, 12978−12983.
77. Weiss, M. A., Hua, Q. X., Jia, W., Nakagawa, S. H., Chu, Y. C., and Katsoyannis, P. G. (2002) in *Insulin & Related Proteins: Structure to Function and Pharmacology* (Dieken, M. L., Federwisch, M., and De Meyts, P., Eds.) pp 103−119, Kluwar Academic Publishers, Dordrecht, The Netherlands.
78. Luo, R. Z., Beniac, D. R., Fernandes, A., Yip, C. C., and Ottensmeyer, F. P. (1999) Quaternary structure of the insulin-insulin receptor complex, *Science 285*, 1077−1080.
79. Ottensmeyer, F. P., Beniac, D. R., Luo, R. Z., and Yip, C. C. (2000) Mechanism of transmembrane signaling: Insulin binding and the insulin receptor, *Biochemistry 39*, 12103−12112.
80. Shoelson, S. E., Lee, J., Lynch, C. S., Backer, J. M., and Pilch, P. F. (1993) Bpa^{B25} insulins. Photoactivatable analogues that quantitatively cross-link, radiolabel, and activate the insulin receptor, *J. Biol. Chem. 268*, 4085−4091.
81. Kobayashi, M., Ohgaku, S., Iwasaki, M., Maegawa, H., Shigeta, Y., and Inouye, K. (1982) Supernormal insulin: [D-Phe^{B24}]-Insulin with increased affinity for insulin receptors, *Biochem. Biophys. Res. Commun. 107*, 329−336.
82. Mirmira, R. G., and Tager, H. S. (1989) Role of the phenylalanine B24 side chain in directing insulin interaction with its receptor: Importance of main chain conformation, *J. Biol. Chem. 264*, 6349−6354.
83. Wang, Q. Q., Feng, Y. M., and Zhang, Y. S. (1996) Studies on receptor binding site of insulin: the hydrophobic B12Val can be substituted by hydrophilic thr, *Biochem. Mol. Biol. Int. 39*, 1245−1254.
84. Hua, Q.-X., Hu, S. Q., Jia, W., Chu, Y.-C., Burke, G. T., Wang, S. H., Wang, R. Y., Katsoyannis, P. G., and Weiss, M. A. (1998) Mini-proinsulin and mini-IGF-I: Homologous protein sequences encoding non-homologous structures, *J. Mol. Biol. 277*, 103−118.
85. Markussen, J., Jorgensen, K. H., Sorensen, A. R., and Thim, L. (1985) Single chain *des*-(B30) insulin. Intramolecular crosslinking of insulin by trypsin catalyzed transpeptidation, *Int. J. Pept. Protein Res. 26*, 70−77.
86. Cutfield, J., Cutfield, S., Dodson, E., Dodson, G., Hodgkin, D., and Reynolds, C. (1981) Evidence concerning insulin activity from the structure of a cross-linked derivative, *Hoppe-Seyler's Z. Physiol. Chem. 362*, 755−761.
87. Nakagawa, S. H., and Tager, H. S. (1989) Perturbation of insulin-receptor interactions by intramolecular hormone cross-linking. Analysis of relative movement among residues A1, B1, and B29, *J. Biol. Chem. 264*, 272−279.
88. Lee, H. C., Kim, S. J., Kim, K. S., Shin, H. C., and Yoon, J. W. (2000) Remission in models of type 1 diabetes by gene therapy using a single-chain insulin analogue, *Nature 408*, 483−488.
89. Olsen, H. B., Ludvigsen, S., and Kaarsholm, N. C. (1998) The relationship between insulin bioactivity and structure in the NH_2-terminal A-chain helix, *J. Mol. Biol. 284*, 477−488.
90. Hua, Q.-X., Chu, Y.-C., Jia, W., Phillips, N. F. B., Wang, R.-Y., Katsoyannis, P. G., and Weiss, M. A. (2002) Mechanism of insulin chain combination. Asymmetric roles of A-chain α-helices in disulfide pairing, *J. Biol. Chem. 277*, 43443−43453.
91. Adams, T. E., Epa, V. C., Garrett, T. P. J., and Ward, C. W. (2000) Structure and function of the type 1 insulin-like growth factor receptor, *Cell. Mol. Life Sci. 57*, 1050−1093.

92. Peitsch, M. C., Herzyk, P., Wells, T. N., and Hubbard, R. E. (1996) Automated modelling of the transmembrane region of G-protein coupled receptor by Swiss-model, *Receptors Channels 4*, 161−164.
93. Mynarcik, D. C., Yu, G. Q., and Whittaker, J. (1996) Alanine-scanning mutagenesis of a C-terminal ligand binding domain of the insulin receptor α subunit, *J. Biol. Chem. 271*, 2439−2442.
94. Kristensen, C., Wiberg, F. C., Schaffer, L., and Andersen, A. S. (1998) Expression and characterization of a 70-kDa fragment of the insulin receptor that binds insulin. Minimizing ligand binding domain of the insulin receptor, *J. Biol. Chem. 273*, 17780−17786.
95. Fabry, M., Schaefer, E., Ellis, L., Kojro, E., Fahrenholz, F., and Brandenburg, D. (1992) Detection of a new hormone contact site within the insulin receptor ectodomain by the use of a novel photoreactive insulin, *J. Biol. Chem. 267*, 8950−8956.
96. Luo, Y., and Baldwin, R. L. (1999) The 28−111 disulfide bond constrains the α-lactalbumin molten globule and weakens its cooperativity of folding, *Proc. Natl. Acad. Sci. U.S.A. 96*, 11283−11287.
97. Pierce, S. B., Costa, M., Wisotzkey, R., Devadhar, S., Homburger, S. A., Buchman, A. R., Ferguson, K. C., Heller, J., Platt, D. M., Pasquinelli, A. A., Liu, L. X., Doberstein, S. K., and Ruvkun, G. (2001) Regulation of DAF-2 receptor signaling by human insulin and ins-1, a member of the unusually large and diverse *C. elegans* insulin gene family, *Genes Dev. 15*, 672−686.
98. Banner, D. W., D'Arcy, A., Janes, W., Gentz, R., Schoenfeld, H. J., Broger, C., Loetscher, H., and Lesslauer, W. (1993) Crystal structure of the soluble human 55 kd TNF receptor-human TNF β complex: Implications for TNF receptor activation, *Cell 73*, 431−435.
99. Postel-Vinay, M. C., and Kelly, P. A. (1996) Growth hormone receptor signaling, *Bailliere's Clin. Endocrinol. Metab. 10*, 323−336.
100. Castellino, A. M., and Chao, M. V. (1996) Trans-signaling by cytokine and growth factor receptors, *Cytokine Growth Factor Rev. 7*, 297−302.
101. Goffin, V., and Kelly, P. A. (1997) The prolactin/growth hormone receptor family: Structure/function relationships, *J. Mammary Gland Biol. Neoplasia 2*, 7−17.
102. Livnah, O., Stura, E. A., Middleton, S. A., Johnson, D. L., Jolliffe, L. K., and Wilson, I. A. (1999) Crystallographic evidence for preformed dimers of erythropoietin receptor before ligand activation, *Science 283*, 987−990.
103. Chu, Y. C., Burke, G. T., Gammeltoft, S., Chan, S. J., Steiner, D. F., and Katsoyannis, P. G. (1994) High-potency hybrid compounds related to insulin and amphioxus insulin-like peptide, *Biochemistry 33*, 13087−13092.
104. Li, M., Cui, D., and Zhang, Y. (2002) Isosteric replacement of A3 Val of porcine insulin by *allo*-Thr, *IUBMB Life 53*, 57−60.
105. Weiss, M. A., Wan, Z., Zhao, M., Chu, Y. C., Nakagawa, S. H., Burke, G. T., Jia, W., Hellmich, R., and Katsoyannis, P. G. (2002) Non-standard insulin design: Structure−activity relationships at the periphery of the insulin receptor, *J. Mol. Biol. 315*, 103−111.
106. De Meyts, P. (2002) Insulin and insulin-like growth factors: The paradox of signaling specificity, *Growth Horm. IGF Res. 12*, 81−83.
107. Weiss, M. A., Nakagawa, S. H., Jia, W., Xu, B., Hua, Q. X., Chu, Y. C., Wang, R. Y., and Katsoyannis, P. G. (2002) Protein structure and the spandrels of San Marco: Insulin's receptor-binding surface is buttressed by an invariant leucine essential for protein stability, *Biochemistry 41*, 809−819.
108. Brader, M. L., and Dunn, M. F. (1991) Insulin hexamers: New conformations and applications, *Trends Biochem. Sci. 16*, 341−345.
109. Brange, J. (1987) *Galenics of insulin: The physico-chemical and pharmaceutical aspects of insulin and insulin preparations*, Springer-Verlag, Berlin.
110. Weiss, M. A., Hua, Q. X., Lynch, C. S., Frank, B. H., and Shoelson, S. E. (1991) Heteronuclear 2D NMR studies of an engineered insulin monomer: Assignment and characterization of the receptor-binding surface by selective ^{2}H and ^{13}C labeling with application to protein design, *Biochemistry 30*, 7373−7389.
111. Cosmatos, A., Cheng, K., Okada, Y., and Katsoyannis, P. G. (1978) The chemical synthesis and biological evaluation of [1-L-alanine-A]- and [1-D-alanine-A]insulins, *J. Biol. Chem. 253*, 6586−6590.
112. Geiger, R., Geisen, K., Regitz, G., Summ, H. D., and Langner, D. (1980) Insulin analogues with substitution of A1-glycine by D-amino acids and ω-amino acids, *Hoppe-Seyler's Z. Physiol. Chem. 361*, 563−570.
113. Wan, Z. L., and Liang, D. C. (1990) Studies on the crystal structure of A1-(D-Tryptophan) insulin, *Sci. China B 33*, 810−820.
114. Chothia, C., Lesk, A. M., Dodson, G. G., and Hodgkin, D. C. (1983) Transmission of conformational change in insulin, *Nature 302*, 500−505.
115. DeFelippis, M. R., Chance, R. E., and Frank, B. H. (2001) Insulin self-association and the relationship to pharmacokinetics and pharmacodynamics, *Crit. Rev. Ther. Drug Carrier Syst. 18*, 201−264.
116. Ciszak, E., Beals, J. M., Frank, B. H., Baker, J. C., Carter, N. D., and Smith, G. D. (1995) Role of C-terminal B-chain residues in insulin assembly: The structure of hexameric $Lys^{B28}Pro^{B29}$-human insulin, *Structure 3*, 615−622.
117. Zhao, M., Nakagawa, S. H., Hua, Q. X., and Weiss, M. A. (1998) Exploring the foldability and function of insulin by combinatorial peptide chemistry, *Proc. Am. Pept. Symp.*, 369−371.
118. Bi, R. C., Dauter, Z., Dodson, E., Dodson, G., Giordano, F., and Reynolds, C. (1984) Insulin structure as a modified and monomeric molecule, *Biopolymers 23*, 391−395.
119. Dai, J.-B., Lou, M.-Z., You, J.-M., and Liang, D.-C. (1987) Refinement of the structure of despentapetide (B26−B30) insulin at 1.5 Å resolution, *Sci. Sin. 30*, 55−65.
120. Cockram, C. S., Jones, R. H., Sonksen, P. H., Tatnell, M. A., Zhu, S. Q., and Dodson, G. (1987) An examination of the role of insulin dimerisation and negative cooperativity using the biological properties of the despentapeptide and deshexapeptide insulins, *Diabetologia 30*, 733−738.
121. Doyle, A. C. (1953) "Silver Blaze" in *The Complete Sherlock Holmes*, vol. 1, p. 397, Doubleday & Co., New York.

BI047585K